Shell closure, magic and exotic nuclei

Olivier Sorlin
Grand Accélérateur National d'Ions Lourds (GANIL), CEA/DSM-CNRS/IN2P3
B.P. 55027, F-14076 Caen Cedex 5, France

ABSTRACT :

The advent of Radioactive Ion Beam facilities worldwide has progressively modified our vision and interpretation of the shell evolutions. Indeed it has become possible to explore the evolution of shell gaps for a large range of isotopes or isotones, hereby exploring various properties of the nuclear interactions such as spin or central dependences. Parallel to experimental breakthroughs, considerable progresses are being achieved to derive an in-medium nuclear force from bare the nucleon-nucleon interactions. The role of the tensor and three body forces, the origin of the spin-orbit interaction and the influence of the continuum of states are modern aspects of fundamental importance that are currently under investigation.

The present lecture, given at the 2009 International Joliot-Curie school (EJC2009), focuses on the evolution of shell closures and magic nuclei. A special emphasis is to understand which properties of the nucleon-nucleon forces can modify the structural evolution, as it is observed experimentally. The manuscript is organized in five parts. The first part reminds the basics concepts of the atomic nucleus, the second gives the main features of the in-medium nucleon-nucleon interaction. It is followed by two parts dedicated to the evolution of the N=20 and N=28 shell closures. Finally implication of the nuclear force properties to nuclear astrophysics will be introduced in connection with the astrophysical rapid neutron capture process at the N=82 shell closure. The present lecture has great synergies with others given in the school, as in particular with the work of N. Smyrnova which focuses more on the theoretical aspects of the shell evolution viewed from the Shell Model point of view.

Contents

INTRODUCTION

Our vision of the magic numbers up to the 70's was guided by the paucity of experimental information away from stable nuclei. The systematically large drops of n or p separation energies after having passed major shell gaps, the high energy and weak excitation probabilities of the first excited states of magic nuclei, give rise to the assumption that the so far discovered magic shells were persisting throughout the whole chart of nuclides. With the technical possibility of exploring nuclei with increasingly large N/Z ratios, the persistence of the N=20 shell gap was first examined in the 70's using atomic masses, radii and spectroscopic information. These combined results provided first evidence that magic numbers were not immutable, and triggered a large number of experimental and theoretical works devoted to search for the disappearance of magic shells and their origin. This pioneering work also called for the development of radioactive beam facilities worldwide. Nowadays, our vision is enlarged, as shown with the large blue and red coloured regions in the chart of nuclides in Figure 1. The stable nuclei in black reside in the valley of stability and those far from this valley are called 'exotic'. This word echoes the search of exotic lands by our ancestors.

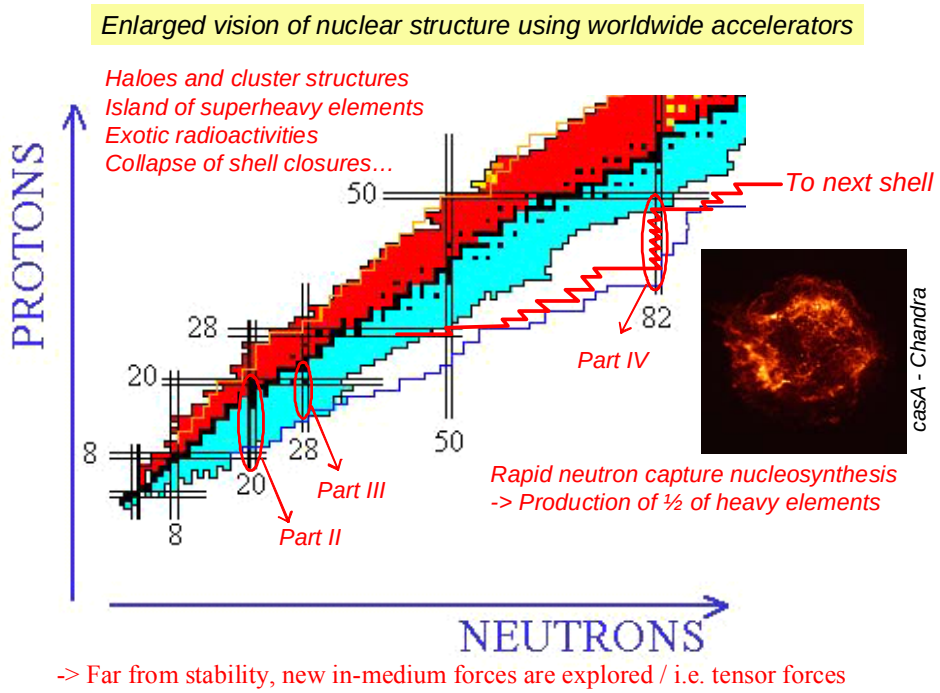

Figure 1: View of the chart of nuclides showing the valley of stability (black), as well as neutron-rich (blue) and neutron deficient (red) nuclei. The N=20, 28 and N=82 regions, which will be studied in this lecture, are shown in the ellipsoidal areas.

Part I of this manuscript will present the basic concepts of the atomic nucleus, Part II the main features to be known in nuclear physics to address the shell evolution driven by nuclear forces. Part III will illustrate the role of nuclear forces to account for the reduction of the N=20 gap, while Part IV will focus on the physics at the N=28 shell closure far from stability. At the end of these chapters we shall try to find universal trends which take root in the properties of the NN forces that can be applied in unknown regions of the chart of nuclides, as for the evolution of the N=82 shell closure. This shell closure is playing a key role in producing the heavy elements in the universe from slow (s process) or rapid (r process) neutron-capture nucleosynthesis. Implications of the nuclear structure evolution to astrophysics will be developed in Part V.

PART I: BASIC CONCEPTS OF THE ATOMIC NUCLEUS

The atomic nucleus, a world apart

The modelling of the atomic nucleus requires handling strong short range interactions between N constituents, which is not solvable analytically. Fortunately, but also paradoxically, the Mean Field (MF) approach can be used to treat medium and heavy mass systems. This is mainly due to the Pauli principle which excludes the scattering of fermions to states already occupied by others, making the nuclear core rather inert. Ab initio methods are so far limited to lighter nuclei, mainly as they require huge computational power. In the MF framework, one assumes that each nucleon encounter a mean field created by all others. Model used nowadays in nuclear physics are largely guided by experimental observations. In the 60's, electron scattering measurements allow to deduce the shape of the MF potential from the charge density of the nucleus, while the irregular spacing of the orbits due to shell gaps was deduced from (e,e',p) studies.
The shell model uses the single particle energies derived from a closed core nucleus and a set of effective or 'dressed' two body matrix elements to model excitations that are occurring within a given valence space. These 'in-medium' two-body interactions (or 'effective' interactions) differ from the ones obtained from the free scattering of nucleons (or 'bare' forces) as they intrinsically contain some amount of interaction from the core or contain three body forces. One major challenge in our domain is therefore to bridge from free (or bare) NN interaction to the in-medium value. Such comparisons have revealed in particular that *three body* interactions are required to account for the building of the major shell gaps.

The uniqueness of the atomic nucleus as a quantum system is that (i) it creates his own potential, contrary to electrons in atoms which feel the MF potential created by the protons of the nucleus (ii) the nucleus is composed of two proton and neutron quantum fluids, (iii) single nucleon excitations mix with collective modes such as vibrations or rotations already at modest excitation energy.

The growing possibility of exploring large N/Z ratios in the atomic chart of nuclides is continuously bringing promises and discoveries of new phenomena, such as halo or cluster structures, exotic shapes, an island of superheavy nuclei, change of major shell closures and appearance of new ones. Once major shell gaps are weakened, cross shell excitations can develop. There, nucleons from occupied shells move to valence ones giving rise to particle-hole excitations. When several coherent particle-hole excitations modes are involved, the nucleus can no longer be considered as composed of independent nucleons but behaves rather as a collective vibrator or rotor. This passage from independent to strongly coherent motions is also an interesting issue in quantum physics, which manifests clearly in atomic nuclei.

Charge distribution and shell structure viewed from electron scattering

Electrons are ideal probes to determine the charge density of nuclei, as electrons interact solely through the well known Coulomb field with protons and not through strong nuclear forces. At suitable energies, given by the relation $E_e = \hbar c/\lambda\!\!\!^{-}$, they are used to determine the charge density profile ρ(r) of various nuclei using stable targets. A high resolution spectrometer is used to determine the transferred momentum **q** encountered during their Coulomb interaction while traversing the nucleus. The density distribution, shown in the bottom part of Figure 2, correspond approximately to the inverse Fourier transform of the momentum distribution F(q) shown in the top part of the Figure. The F(q) pattern looks analogous to Airy function obtained in optics by the diffusion from a semi-transparent object. Large **q** values give access to the central density part, while small **q** values inform on the surface shape, i.e. F(q) scales with the mean square radius value $\langle r \rangle^2$. Various stable nuclei have been studied with this technique, and it was deduced that the charge radius varies as $A^{1/3}$, meaning that the volume of nuclei scale with A. This scaling factor confirms the saturation property of nuclear forces, i.e. a constant central density value with increasing A. So far, these studies can be achieved with stable target only, and the change in density surface with large N/Z (increased diffuseness for instance) or the occurrence of a depleted central density for unstable nuclei cannot be checked with this technique. Electron-ion colliders are being planned at the SCRIT facility [Waka04] at the RIKEN accelerator to investigate these issues.

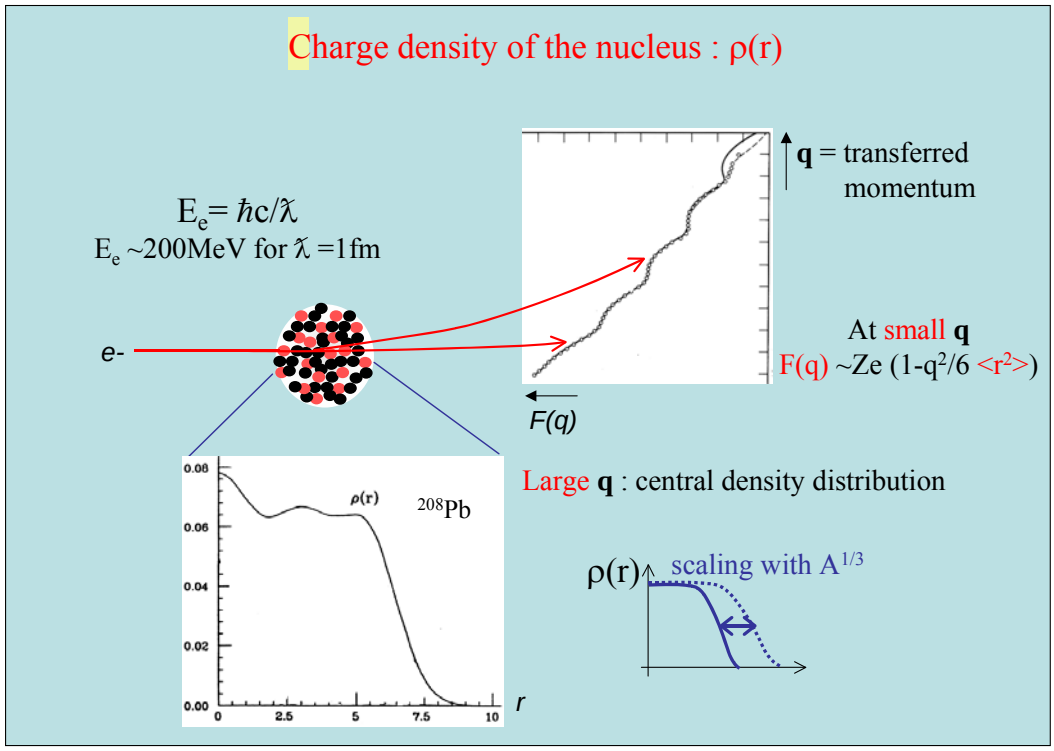

Figure 2: Charge density distribution of the ^{208}Pb nucleus derived from electron scattering [Heis69].

At higher electron energy (typically 500MeV) thinner details of the structure of the atomic nucleus are examined, such as the nucleons themselves. High energy electrons can be used to knock-out individual protons located on the various shells inside the nucleus. This is the (e,e',p) technique illustrated in Figure 3 with a Pb target. There, the proton energies scale with the ones of the orbits they were knocked-out from. Different peaks, labelled as $1/2^+$, $3/2^+$, $11/2^+$ and $5/2^+$, are shown in Figure 3. They correspond to knocked-out protons from the $s_{1/2}$, $d_{3/2}$, $h_{11/2}$, and $d_{5/2}$ orbits. The amplitude of the each peak scales roughly with the expected occupancy of the state which amounts (2J+1) for each. For instance, the signal from the $h_{11/2}$ orbit (which should contain 12 protons) is the largest, while the $s_{1/2}$

which can contain only two protons is about 5 times weaker than the one corresponding to the $h_{11/2}$ orbit. This significant occupancy characterizes states carrying a large fraction of single particle energies. These features show that, at a first approximation, the experimental spectra look like the one expected using a one-body potential with a spin-orbit interaction.
This picture breaks down at higher excitation energy, where correlations beyond the independent particle model must be taken into account. In particular, only a weak fraction of the signal from the $g_{7/2}$ orbit is seen, the remaining part being present at higher excitation energy. Here the $7/2^+$ state at 3.47MeV can partly originate from the coupling of the $h_{11/2}$ with the 3^- state of the ^{208}Pb core nucleus. Other states are present at higher excitation energy. This spreading of the single particle strength is a general feature observed in atomic nuclei. Single excitation energies can mix with collective modes (vibrations or rotations) when the nuclear excitation energy increases. This gives rise to more complex excitation energy spectra to interpret, which require to unfold single particle energy excitations from collective modes. Shell model calculations are good tool to achieve this goal, as it will be exemplified in the following. The independent particle models can be successfully applied around closed shells up to moderate excitation energy. In between closed shells, coupling to collective modes occurs already at low excitation energy.

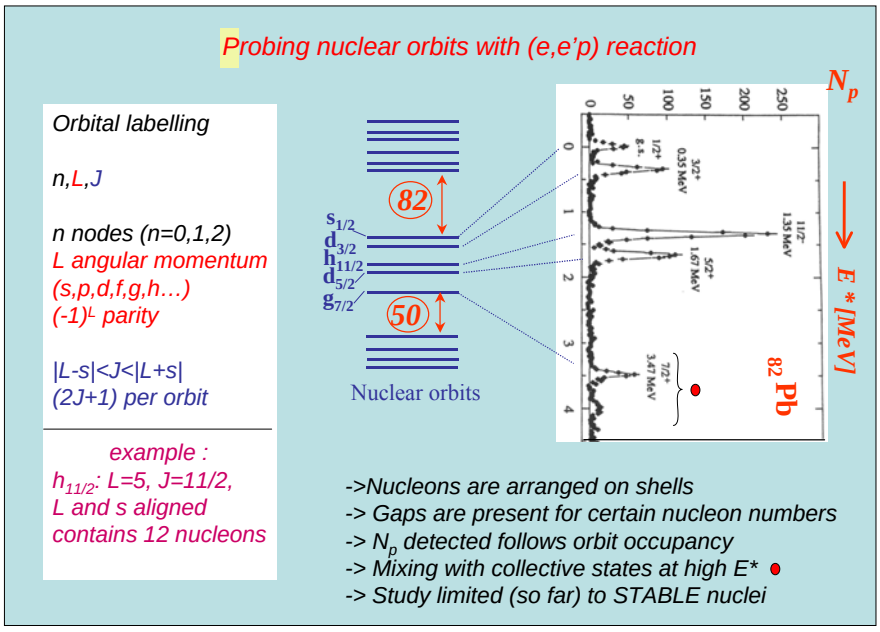

Figure 3: Sequence of proton orbits in the (Z=82) ^{208}Pb nucleus derived from the proton knock-out induced by electrons [Quin86]. Irregular spacing between shells is evidenced. The number of protons N_p per peak scales roughly with the occupancy of the states.

Taking the density distribution deduced from electron scattering, and a simple $-v_0\delta(r-r')$ interaction to simulate the short range of the nuclear interaction, a mean field potential U(r) can be derived using the folding procedure illustrated in Figure 4. In this procedure the mean field U(r) is the integral of the two-body NN interaction over the volume of the nucleus having a charge density $\rho(r')$. It immediately follows that $U(r)= -v_0\rho(r)$ has the same shape as the charge distribution, with an opposite sign. The use of an Harmonic Oscillator (HO) added to an L^2 term (which flattens the potential well at large angular momenta, and hence at large distances), is a good approximation to simulate the MF potential well of a nucleus. Solving the Shrödinger equation, irregular spacing between orbits is found, with large shell gaps at 8, 20 and 40 For heavier nuclei, a spin-orbit (SO) interaction was postulated in 1949 independently by Mayer, Haxel and Suess [May49] to reproduce the observed behaviours associated with the 50, 82 and 126 numbers. At this time a spin-orbit term was introduced in analogy to atomic physics, though its strength in nuclear physics is considerably larger and its origin very different. In nuclear systems the spin-orbit term takes root in the spin dependence of the nuclear interaction itself.

Its origin is now relatively well qualitatively accounted for by relativistic MF theories using the Dirac formalism. Consequently there are mainly two kinds of magic numbers, the ones generated by the HO potential (8, 20, 40) and the others by adding the SO potential (14,28,50,82 and 126), both co-existing in intermediate mass region (A~40) when the SO interaction is not too large (see Figure 4).

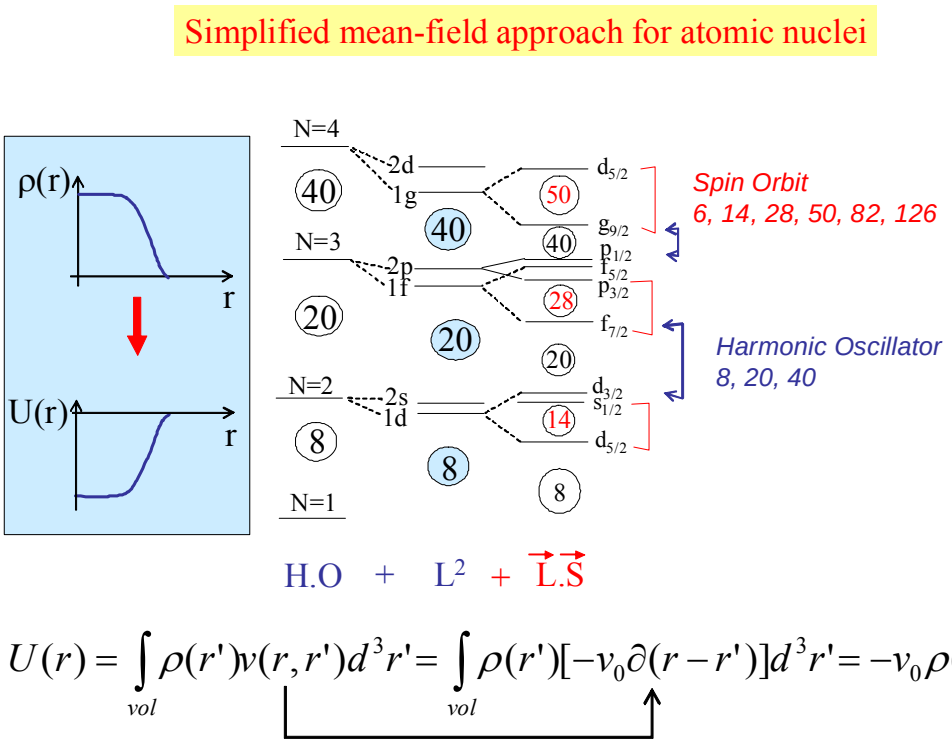

Figure 4: Mean Field potential U(r) derived from a simplified folding potential. Given the shape of the nuclear charge density, a harmonic oscillator + L^2 term is often used as a starting mean field approximation. From this, the N=28, 20 and 40 shell closures are found. The addition of a spin-orbit potential enables to reproduce the observed N=14,28,50,82 and 126 shell gaps.

These two kinds of closed shells (which have different origins) will be studied separately in the following. The characteristics of the two associated shell gaps are:

- For a HO gap, orbits located above and below the gap have opposite parities (at N=20 : $d_{3/2}$ has L=2 and parity + while $f_{7/2}$ has L=3 with parity -). It follows that quadrupole excitations which preserve the parity symmetry are forbidden at the one particle - one hole (1p1h) level, while they are permitted and efficient at the 2p2h level to generate collectivity.
- Gaps created by the SO interaction involve orbits of the same parity, separated by two units of angular momentum (N=28 is formed between the $f_{7/2}$ and $p_{3/2}$ orbits that have both a negative parity, and are separated by 2 units of angular momentum ΔL=2). These features naturally favour quadrupole excitations (characterized by ΔL=2) already at the 1p1h level.

This casting of magic numbers in two categories renders the study of the evolution magic numbers more general and prevents from the necessity of making an exhaustive catalogue of the behaviour of all existing shell gaps. Rather we focus on the two shell gaps 20 and 28, which are prototypical cases of HO and SO-like shell gaps, respectively. Analogies and expected trends for other shell closures will be discussed briefly at the end of sections III and IV. The reader interested by more details related to other shells can refer to the review article [Sorl08].

Take away message – Part I

Key features on the basic concepts of the atomic nucleus

The study of nuclear charge density from electron scattering has shown:

- The constancy of the central nuclear density as the nucleus grows in size due to the saturation property of the nuclear forces

- The scaling of the nuclear charge radius with $A^{1/3}$

- Using a folding procedure, it is found that the mean field potential has the shape of the charge distribution, with opposite sign

The observation of individual orbits in closed shell nuclei has shown that:

- In a first approximation nucleons can be considered as independent particles, occupying single particle states

- A fragmentation of the single particle strength occurs at high energy for closed-shell nuclei, and lower for mid-shell nuclei, emphasizing the role of correlations to describe the energy spectrum of nuclei

- The nuclear shell gaps exhibit HO+L^2 (N=8,20,40) or LS (6, 14, 28, 50, 82, 126) patterns which have different properties with respect to parity conservation and quadrupole symmetry

Part II: MAIN PROPERTIES OF THE IN-MEDIUM NN INTERACTION

Modifications of shell gaps take root in the properties of nuclear forces. Therefore, before addressing the shell gap changes, it is worth to remind some properties of the nuclear forces. To a first approach one can simply understand some of the qualitative properties of the in-medium nucleon-nucleon (NN) interaction as their quantitative values are more often empirically deduced from the observed properties of nuclei. Attempts are being made nowadays to deduce in-medium properties from the bare forces obtained from nucleon-nucleon scattering experiments. However as discussed for instance in the lectures of D. Lacroix, T. Duguet, this is not a trivial procedure.

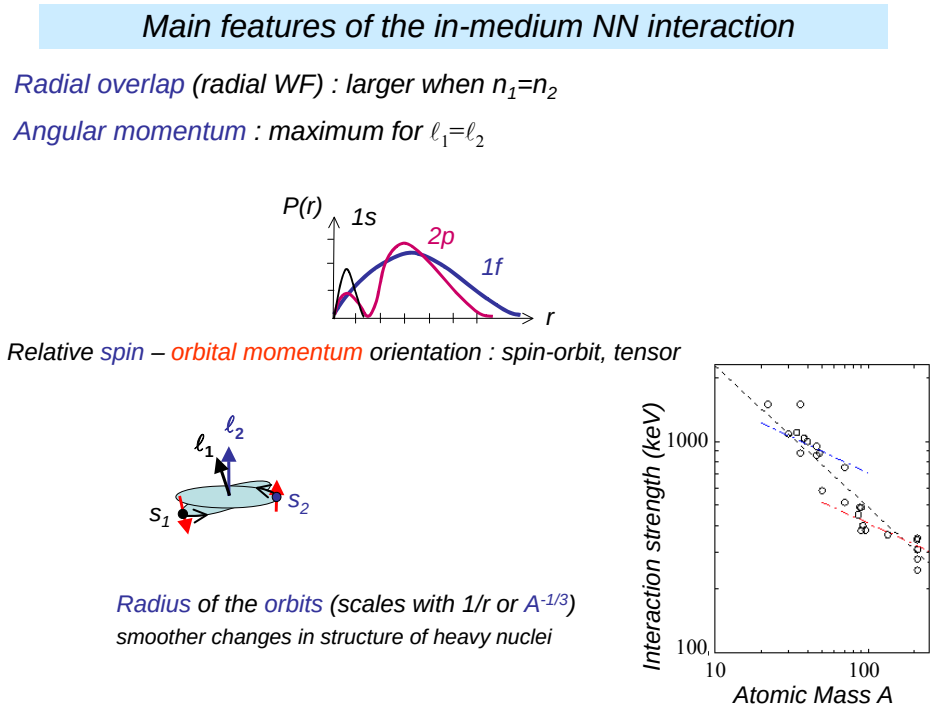

Figure 5: Main properties of the in-medium nucleon-nucleon interaction. It varies with the radial overlap of the wave function of the constituents, and is the largest when the two nucleons have similar angular momenta. It depends on the relative spin and orbital momentum orientation of the interacting nucleons and is reduced from about 1.5MeV at A~20 to 250KeV at A~200, as shown in the bottom right picture (see text for more details).

Some of the fundamental useful properties of the nucleon-nucleon interaction are listed below:

- Reminding that a nucleon wave function (WF) can be characterized by the n, ℓ and j quantum numbers, n being number of nodes, ℓ and j the orbital and total angular momenta, one can easily understand that a stronger interaction is found when the WF of two nucleons spatially overlap strongly. This is favoured for WF having the same number of nodes n, and/or the same angular orbital momentum value ℓ.
- The nuclear interaction is spin-dependent, in particular the proton-neutron interaction is larger between protons and neutrons having anti-aligned spin configurations, i.e. between $j_1>$ and $j_2<$, where $j_1>$ is the higher component of the ℓ_1 s_1 coupling and $j_2<$ the lower component of the ℓ_2 s_2 coupling. For instance the proton neutron $d_{5/2}d_{3/2}$ interaction is larger than the $d_{5/2}d_{5/2}$ one.
- Empirically, it is found that the strength of in-medium interactions scales with the inverse size of the nucleus, that is to say with $A^{-1/3}$ or $A^{-2/3}$, depending if the WF of the nucleons are located rather at the surface or in a slightly more central surface ring. This is derived from the experimental values of the NN interactions reported as open circles in the bottom right part of Figure 5. Indeed, this scaling originates from the fact that as the nucleus grows in size, the strength of the interaction between two nucleons becomes reduced, as the nucleons rarely 'see' each others given the short range of the nuclear interaction. The dashed and dashed dotted lines correspond to the $A^{-1/3}$ and

$A^{-2/3}$ trends, respectively. An important consequence of this decrease with increasing A is that a *modification of shell structure is expected to be faster in light systems* (having large absolute interaction strengths) *than in heavier ones*.

- As the nucleus is composed of protons and neutrons there exists two values of isospin T=0 (exclusively between unlike particles) and T=1 which exist both for like and unlike particles. This latter feature makes the proton-neutron (pn) interaction effectively stronger than the neutron-neutron (nn) or proton-proton (pp) ones, despite the nuclear interaction is almost charge independent. It follows that shell modifications and the onset of deformation are often triggered by pn interactions.

Empirical determination of proton-neutron interactions from odd-odd nuclei

The strength of a given proton-neutron interaction can be determined experimentally from the known spectroscopy of odd-Z odd-N nuclei. In the present example, the proton-neutron $d_{3/2}$-$f_{7/2}$ interaction V^{pn} is inferred assuming a closed core nucleus of ^{36}S to which one proton is added in the $d_{3/2}$ orbit and one neutron in the $f_{7/2}$ one, leading to the ^{38}Cl nucleus[1]. For this purpose we determine first the binding energy (BE) obtained by adding independently one proton in the $d_{3/2}$ orbit (using the BE of ^{37}Cl, labelled as S_p in Figure 6) and one neutron in the $f_{7/2}$ orbit (using the BE of ^{37}S, or S_n in Figure 6).

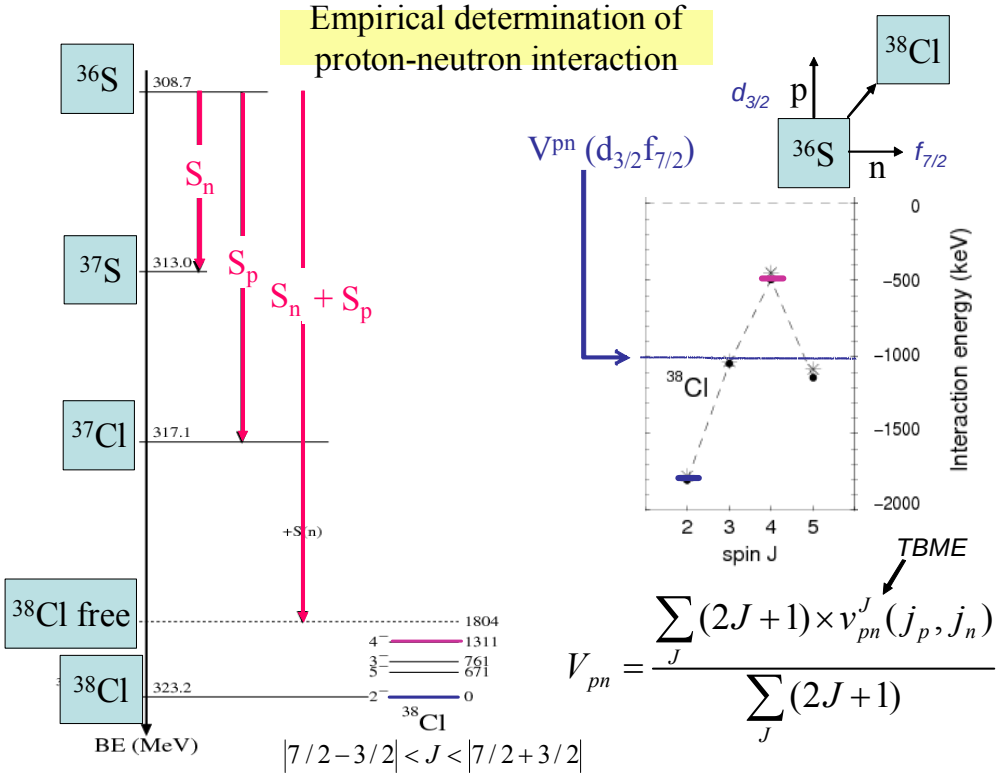

Figure 6: Experimental binding energies of the ^{36}S, ^{37}S, ^{37}Cl and ^{38}Cl nuclei are used to infer the interaction energy between one valence proton in the $d_{3/2}$ and one valence neutron in the $f_{7/2}$ orbitals. The interaction energy $v^J(j_p,j_n)$ is represented in the right part of the figure. It is given by the TBME associated with the coupling of 2 nucleons to J=2-5. The (2J+1) weighted average value of this interaction energy correspond to the mean corresponding proton-neutron interaction (horizontal line at about -1000keV), also called the monopole interaction V^{pn}.

[1] This assumption of a purely closed and inert core is helpful to understand the underlying concept of proton-neutron interaction. However, in reality these valence nucleons interact with the core nucleons. Therefore the deduced two-body interaction energies and the monopole term derived from this method should not be directly compared with the ones obtained from bare NN interactions.

Adding these two terms, we obtain a BE value consisting of one p and one n NOT bound, or free, in the ^{38}Cl nucleus, i.e. BE(^{38}Cl$_{free}$)= BE(^{36}S)+S$_n$(^{37}S)+S$_p$(^{37}Cl). We compare this value to the experimental BE's of the J=2,3,4,5 states in ^{38}Cl obtained by the coupling of a $d_{3/2}$ proton and a $f_{7/2}$ neutron (J_{min}= (7/2 - 3/2)= 2; J_{max} = (7/2 + 3/2) =5). The experimental ground state of ^{38}Cl corresponds to J=2$^-$, which is bound by 1804keV as compared to BE(^{38}Cl$_{free}$) obtained by adding freely one proton and neutron to a ^{36}S core. Assuming that the extra binding energy is solely due to the extra proton and neutron, we obtain interaction energies of $\nu^J(j_p,j_n)$ = BE(^{38}Cl$_{free}$) - BE(^{38}Cl)^J for the different J states. For J=3,4,5 weaker interaction energies are obtained as shown in the right hand side of Figure 6. The interaction energy could be fitted as a function of J by using a multipole expansion. The first term is the weighted interaction energy value. It is denoted as V^{pn} in Figure 6 and is called the **monopole energy**. It amounts to -1MeV in the present case. The second term of the multipole expansion is the quadrupole, it is responsible for the parabolic curvature of the function. Monopole interactions have very important impact on the evolution of the nuclear structure, while quadrupole interactions do play a role for correlations. The monopole interaction represents the mean change in binding energy due to given in medium NN interactions and thus represents the leading factor towards shell gap changes. Some of them can be determined experimentally using the method described here, in particular near closed shell nuclei. But this determination requires many constraints which are not often fulfilled: a well closed shell core should be found (A,Z), none of the nuclei involved (A+1,A+2) in the calculation should be deformed, all the components of the multiplet of states should be known experimentally. This latter feature is often hard to obtain, as nuclear states of low and high spin values often require different experimental techniques to be identified. Coming back to our example, it follows that keeping the assumption of an inert core valid, the addition of $d_{3/2}$ protons to ^{36}S will bind the neutron $f_{7/2}$ orbit by about 1MeV per proton added. This can be checked by looking at the neutron binding energy systematic with increasing proton number in Figure 7.

Empirical determination of proton-neutron interactions from binding energy curves

It was mentioned earlier that around closed shells, low energy nuclear states are rather pure single particle states as core excitations which are located at higher energies do not couple with these individual nucleon excitations. Therefore evolutions of the neutron binding energies of the 7/2$^-$ and 3/2$^+$ states shown in Figure 7 should correspond approximately to the energy change of the $f_{7/2}$ and $d_{3/2}$ orbits, respectively. Within the shell model approach the use of *effective* single particle energies **(ESPE)** is useful. It corresponds to the variation of the binding energies induced by the monopole interactions solely. Therefore, for nuclei in the vicinity of closed shells, the experimental binding energy is similar to the ESPE value, while for nuclei containing major correlations such as deformed nuclei, this identity is no longer valid. Adding *x* protons in the $d_{3/2}$ orbit, we expect the ESPE of the neutron $f_{7/2}$ orbit $\varepsilon(f_{7/2})$ to be increased *linearly* :

$$\Delta\varepsilon(f_{7/2}) = x \,.V^{pn}\,(d_{3/2}f_{7/2}),$$

where $V^{pn}(d_{3/2}f_{7/2})$ corresponds to the mean proton-neutron binding energy between one proton in the $d_{3/2}$ and one neutron in the $f_{7/2}$ orbital. Taking the value of $V^{pn}(d_{3/2}f_{7/2})$= -1MeV derived above, we find an increase of the neutron $f_{7/2}$ binding of about 4~MeV when 4 protons are added into the $d_{3/2}$ orbit.
This value can be compared to the one obtained using the evolution of experimental neutron binding energy between Z=16 (S$_n$(^{37}S)=4.303MeV) and Z=20 (S$_n$(^{41}Ca)=8.362MeV), when 4 protons are added in the $d_{3/2}$ orbit[2]. Energy difference between these two S_n values amounts to about 4MeV as well. This shows that the two methods using, (i) the spectrum of odd-odd nuclei or (ii) the slope of the binding energies, agree perfectly well here.

[2] The equivalence between ESPE and the experimental binding energy is valid only for nuclei around/at closed shells. Otherwise correlations change the experimental binding energy significantly.

Additive n-p interactions in the ^{36}S region ?

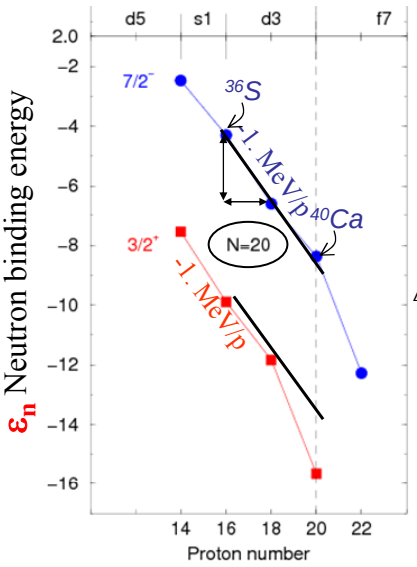

From experiment

From Z=16 to Z=20

$\Delta\varepsilon_n$ (7/2$^-$) ~ 4 V^{pn} ($d_{3/2}f_{7/2}$) ~ -4 MeV

$\Delta\varepsilon_n$ (3/2$^+$) ~ 4 V^{pn} ($d_{3/2}d_{3/2}$) ~ -4 MeV

$$\Delta(20) = \underbrace{(2j_p+1)}_{4}(V^{pn}_{d3/2f7/2} - V^{pn}_{d3/2d3/2}) \sim 0$$

The N=20 shell gap is unchanged !

For nuclei around closed shells

ε_n = Neutron Effective Single Particle Energy

Figure 7: Experimental neutron binding energies as a function of the proton number Z are shown. The slope of the 7/2$^-$ and 3/2$^+$ curves correspond to the $V^{pn}(d_{3/2}f_{7/2})$ and $V^{pn}(d_{3/2}d_{3/2})$ monopoles, respectively. Remarkable is to see the constancy of the size of the N=20 gap between Z=14 and Z=20, if we leave aside the 3/2$^+$ value used for ^{40}Ca as discussed in the text.

Similarly, the evolution of the neutron $d_{3/2}$ orbit can be obtained empirically from the change of the binding energy of the 3/2$^+$ state between N=16 and N=18, using experimental values $S_n(^{36}S)$=9.889MeV and $S_n(^{38}Ar)$=11.838MeV. It can be shown that $V^{pn}(d_{3/2}d_{3/2})$ ~ -1MeV as well. It is therefore found that the slopes of the $d_{3/2}$ and $f_{7/2}$ orbits are similar, due to the fact that the mean nuclear interaction involved have similar intensities, i.e. $V^{pn}(d_{3/2}d_{3/2}) \sim V^{pn}(d_{3/2}f_{7/2})$ [3]. This equal value of nuclear forces has an important consequence on the size of the N=20 shell gap which consequently remains constant between Z=16 and Z=20. We also note that the size of this gap is also the same at Z=14, making the ^{34}Si nucleus an almost doubly magic nucleus. The reader may ask why the $\varepsilon_n(d_{3/2})$ data point at Z=20 (i.e. at ^{40}Ca) is lower than expected. This nucleus having equal number of protons and neutrons, the binding energy of the $d_{3/2}$ neutron is enhanced by the so-called Wigner energy which gives extra binding energies for all N=Z nuclei.

[3] In the first monopole $V^{pn}(d_{3/2}d_{3/2})$ the two nucleons have the same angular momentum, contrary to $V^{pn}(d_{3/2}f_{7/2})$. A priori the $V^{pn}(d_{3/2}d_{3/2})$ monopole value should therefore be larger than $V^{pn}(d_{3/2}f_{7/2})$. However, for $V^{pn}(d_{3/2}d_{3/2})$ the two nucleons have the same spin orientation, contrary $V^{pn}(d_{3/2}f_{7/2})$ where nucleons have opposite spin directions. As said earlier this anti-aligned configuration is more bound in nuclei. This compensates the lowering of binding energy due to the change of angular momentum, making these two monopole terms equal in strength.

The role of quadrupole energy in nuclei

Besides the monopole energy, the nucleus can gain quadrupole energy by adopting a spheroidal or elongated shape. For instance in ^{38}Cl, the left hand side of Figure 8 shows that the J=2 configuration, in which p and n have an open scissor orientation (see the pictogram at the bottom of Figure 8 left), is more bound that the mean energy value. The configuration in which p and n have an orthogonal orientation (J=4) is relatively less bound than the mean value. Indeed, while starting to fill a new shell, the experimental binding energy is often found to be greater than the ESPE obtained from the monopole term solely. In practice, as shown in Figure 8, a gain of quadrupole energy occurs when

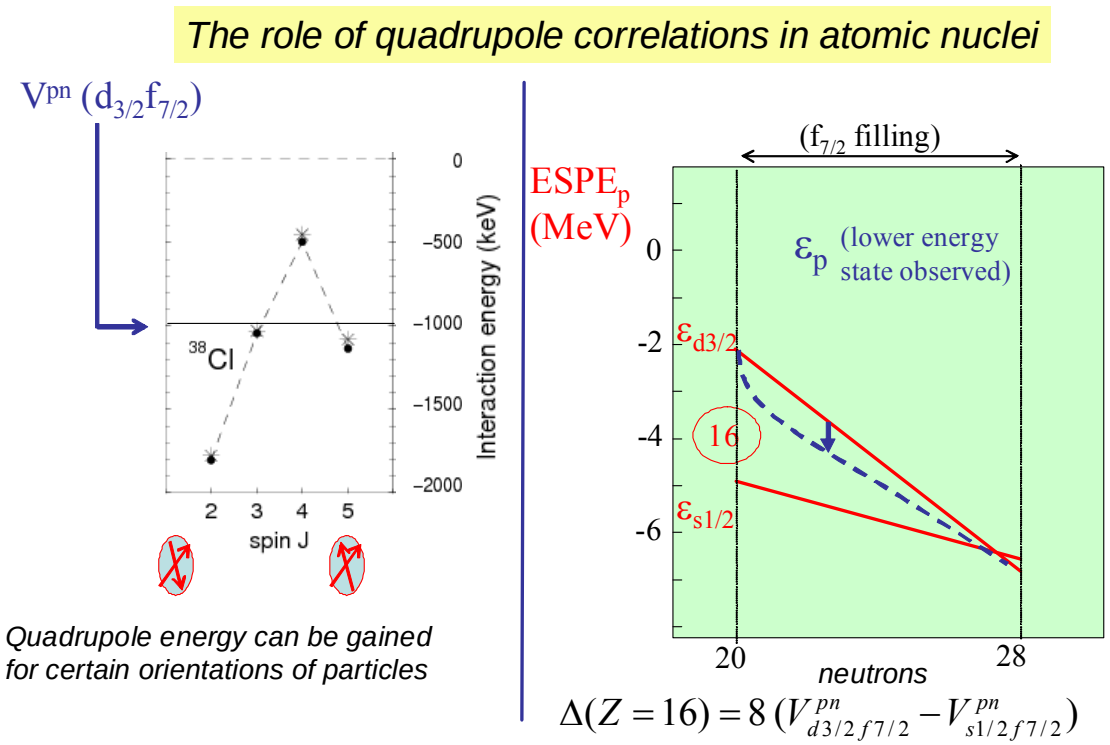

Figure 8: Left : Schematic view of the gain in quadrupole energy obtained by coupling a proton and a neutron in the J=2 configuration (or open scissor orientation). Right : Evolution of the proton Effective Single Particle Energies (ESPE) is shown as a function of the neutron number N using a red full line. Experimental binding energies of the first 3/2$^+$ state are shown with the dashed blue line. The quadrupole gain in energy produces a distortion of the observed binding energy curve to the linear trend obtained from the ESPE values.

starting to fill the $f_{7/2}$ orbit as shown qualitatively with the dashed blue line[4]. Progressively, as the shell gets filled until completeness, this *gain* of quadrupole energy per nucleon vanishes as all magnetic substates (or orientations) which led to a increase in binding energy are already occupied. Then ESPE (full line) and experimental BE (dashed line) converge to reach the same value at each extremes of the shell filling. The overall correlations are maximized at mid shell.

[4] Note here that the evolution of the ESPE of the $d_{3/2}$ proton orbit as a function of the neutron number involves the monopole derived earlier V^{pn} ($d_{3/2}f_{7/2}$).

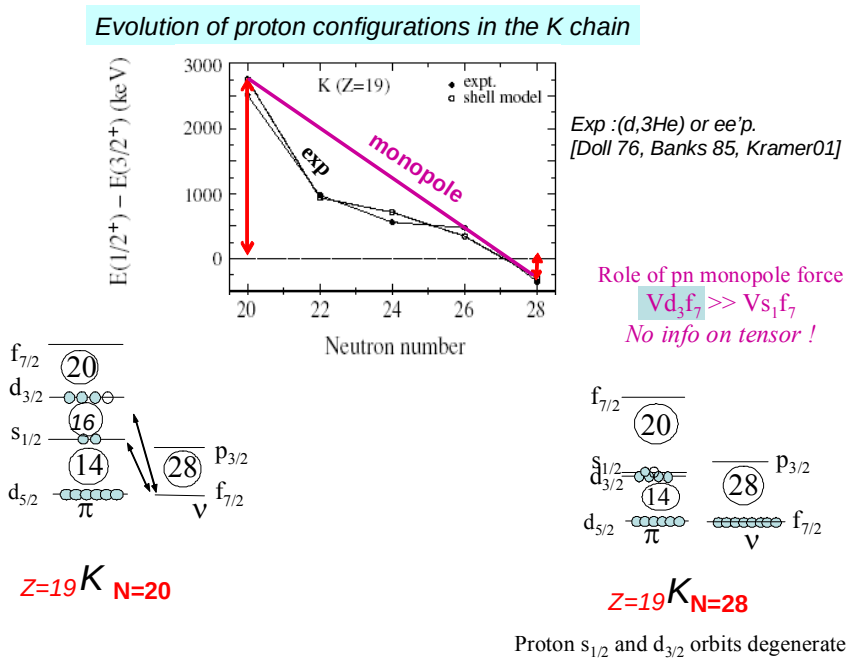

Figure 9: Evolution of $E(1/2^+) - E(3/2^+)$ as a function of neutron number in the $_{19}K$ isotopic chain obtained from (d,^{3}He) and (e,e'p) experiments [Doll76,Bank85,Kram01]. The monopole trend is shown as a linear purple line, while experimental and shell model calculations are shown with filled and open symbols, respectively. The present curve shows that while the neutron $f_{7/2}$ is filled, the $d_{3/2}$ orbit becomes more bound than the $s_{1/2}$ one, hereby breaking the Z=16 sub-shell closure at N=28.

Let us now illustrate the previous statements by looking at the evolution of the *experimental* energy difference between the *first* $1/2^+$ and $3/2^+$ states, $E(1/2^+) - E(3/2^+)$, in the $_{19}K$ isotopic chain as a function of the neutron number. Figure 9 shows data obtained from (d,^{3}He) or (e,e'p) reactions on stable Ca targets [Doll79,Bank85,Kram01,Sorl08]. These reactions enable to probe the proton single particle states in the K chain as well as their occupancy values. At N=21, the proton configuration in the K nucleus is a $d_{3/2}$ hole ($3/2^+$ state), and the first excited is a $s_{1/2}$ hole ($1/2^+$ state). There, the energy difference between these states is of about 2.7 MeV, which approximately corresponds to the size of the Z=16 gap as the $1/2^+$ and $3/2^+$ are almost single particle states. While neutrons fill the $f_{7/2}$ orbit until N=28, this spacing drops to zero and even becomes negative, meaning that the two proton orbits $d_{3/2}$ and $s_{1/2}$ have crossed. We can ascribe this descending trend (straight purple line) to the action of the pn monopole interactions due to the fact that the $V^{pn}(d_{3/2}f_{7/2})$ monopole is more attractive than $V^{pn}(s_{1/2}f_{7/2})$. Deviation of the experimental (exp) and shell model calculations to this linear trend is ascribed to quadrupole or pairing correlations, which lead to an increase of binding energy at mid-shell which vanishes at the two extremes, as mentioned earlier.

The degeneracy of the proton $d_{3/2}$ and $s_{1/2}$ orbits at N=28 has a decisive influence on the onset of proton collectivity at N=28 below ^{48}Ca, as will be discussed later. Keeping this in mind, one should look whether this degeneracy of proton $d_{3/2}$ and $s_{1/2}$ states persists along the N=28 isotones, while removing protons. The results obtained at the NSCL laboratory for ^{45}Cl [Gade06] and ^{43}P [Riley08] allow to put the energy spacing $E(1/2^+) - E(3/2^+)$ in the same viewgraphs for the Cl and P chains, showing a very similar pattern for all in Figure 10[5]. In the P chain the curve is mirror to others as the proton configurations $1/2^+$ and $3/2^+$ in P are particle states with respect to a Z=14 core, while they are hole states in Cl and K with respect to a Z=20 core. By taking the same monopole trend as the one derived in K, the global structural evolution in the Cl and P chains is well reproduced. This emphasizes the robustness of the mechanism and the role of monopole forces there to account for

[5] Note that a similar behavior is observed for $E(5/2^-) - E(3/2^-)$ while filling the neutron $g_{9/2}$ orbit in the $_{29}$Cu isotopic chain [Fran01]. This is caused by a similar a process for which the $V^{pn}(f_{5/2}g_{9/2})$ monopole is more attractive than $V^{pn}(p_{3/2}\, g_{9/2})$.

similar shell evolutions between Z=20 and Z=14. Again correlations are present at mid-shell, leading to the curved pattern (open and filled circles) in between N=20 and N=28, well accounted for by SM calculations. This proximity of $d_{3/2}$ and $s_{1/2}$ shells (separated by 2 units of angular momentum) brings natural quadrupole collectivity around Z=17 at mid proton occupancy of the $d_{3/2}$ and $s_{1/2}$ orbitals. In the P chain, this collectivity is in principle vanishing if the Z=14 is large enough, as $d_{3/2}$ and $s_{1/2}$ shells contain only a single proton. Conversely a reduction of the Z=14 would favor the promotion of $d_{5/2}$ protons to the upper $d_{3/2}$ and $s_{1/2}$ shells. We shall address this point in the following.

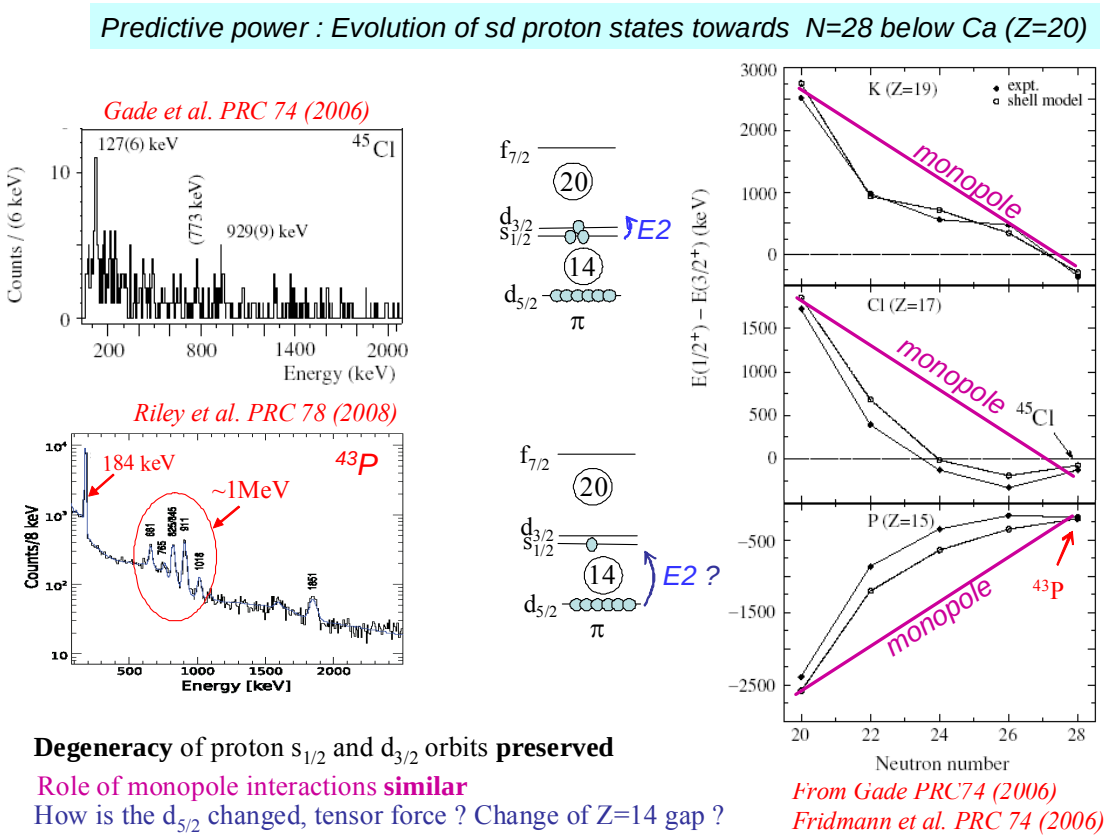

Figure 10: ***Left*** *: Experimental gamma spectra obtained for the N=28, ^{45}Cl (top) and ^{43}P (bottom) nuclei.* ***Right*** *: Evolution of $E(1/2^+) - E(3/2^+)$ as a function of neutron number in the $_{19}$K, $_{17}$Cl and $_{15}$P isotopic chains obtained from experiments using the in-beam spectroscopy using fragmentation reaction [Gade06, Rile08]. The monopole trend is shown as a linear purple line, while experimental and shell model calculations are shown with filled and open symbols, respectively. The curves display the same trend, pointing to a predominant role of the monopole interactions to break the Z=16 sub-shell closure at N=28.*

The evolution of the size of the Z=14 gap can be inferred from experimental data obtained in the S isotopic chain, as shown in Figure 11. At N=20, the ^{36}S(d,^{3}He)^{35}P reaction was used to determine the proton $d_{3/2}$, $s_{1/2}$ and $d_{5/2}$ strengths as a function of excitation energy [Khan85]. In this reaction, large cross sections are obtained for orbits containing a large number of nucleons, which we expect at maximum to be 4, 2 and 6 for the $d_{3/2}$, $s_{1/2}$ and $d_{5/2}$ orbits, respectively. The ground state of ^{35}P is a $1/2^+$ state, and deduced occupancy of the ^{36}S proton state that is presented in the top left part of Figure 11 is close to 2, a value which corresponds to the full occupancy (2J+1)=2 for the (j=1/2, $s_{1/2}$) orbit in the ^{36}S ground state. The first excited state corresponds to the promotion of a proton in the $d_{3/2}$ shell, which is only weakly occupied in ^{36}S as this nucleus has a rather close proton core. The $d_{5/2}$ single particle energy is fragmented in three states from 4MeV to 6MeV which finally collect the full occupancy value of 6 protons for this orbit. This fragmentation occurs because the $d_{5/2}$ orbit is deeply bound. Therefore the $5/2^+$ states are mixed due to coupling with core excitations. Taking the

occupancy weighted energy value of the $5/2^+$ states between 4 and 5.5 MeV, we find an energy value of Z=14 gap of about 5 MeV, while the $d_{3/2}$-$d_{5/2}$ energy spacing amounts to about 7 MeV in ^{36}S.
At N=28, proton knock-out has been carried out at NSCL by Riley et al. [Rile08] to probe the location of the $s_{1/2}$, $d_{3/2}$ and $d_{5/2}$ strengths. Many features deserve comments. First the spectrum of ^{43}P is more compressed than the one of the ^{35}P isotope, pointing to the role of proton-neutron interactions to modify the energy of the proton orbits. Second the $s_{1/2}$ and $d_{3/2}$ orbit are degenerate in energy at N=28, where a gap of more than 2MeV was present at N=20. This confirms the early expectation of the Z=16 collapse. Note that the sum of the occupancies of the two orbits equals to 2, while this occupancy is shared equiprobably between the two $s_{1/2}$ and $d_{3/2}$ orbits which can contain up to 4 and 2 protons, respectively. Third, some $d_{5/2}$ strength is already found at around 1MeV, pointing out to the reduction of the Z=14 gap, and to a much larger fragmentation of the single particle strength. Note that these features are in accordance with the SM calculations of Utsuno [Rile08] or Nowacki [Nowa09], in which tensor forces have been included. These forces lead to a reduction of the Z=14 gap by about 1MeV and of the spacing of the $d_{3/2}$ - $d_{5/2}$ SO partners by about 3MeV. When the neutron $f_{7/2}$, $j_1>$ orbit is filled the tensor part of the nuclear force acts repulsively (attractively) on the $d_{5/2}$,$j_2>$ ($d_{3/2}$, $j_2<$) proton orbits, respectively. Consequently when the neutron $f_{7/2}$ orbit is filled the $d_{3/2}$ one is more bound than without the tensor interaction, while the $d_{5/2}$ is less bound. We shall come back to this important remark later in Parts III and IV.

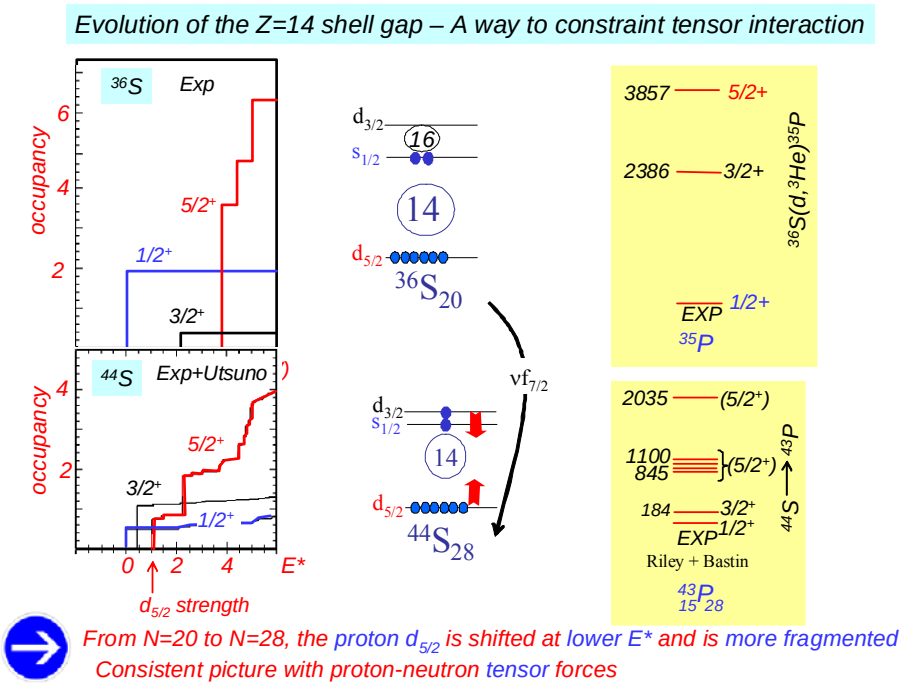

Figure 11: ***Left*** *: Occupancies of the $d_{3/2}$, $s_{1/2}$ and $d_{5/2}$ orbits in the ^{36}S and ^{44}S nuclei. Experimental values in the ^{44}S nucleus extend up to 2MeV. Above 2MeV, the red curve is obtained from the shell model calculations of Utsuno [Rile08]. The good agreement between experimental and calculated values up to 2MeV gives relative confidence in the extrapolation to the highest energy part.* ***Right*** *: Experimental energies of the first excited states in $^{35}P_{20}$ and $^{43}P_{28}$ nuclei obtained from the ^{36}S(d,^{3}He)^{35}P [Khan85] and ^{44}S(-1p)^{43}P [Rile08] reactions, respectively. Note that the level scheme of ^{43}P is much more compressed in energy than the ^{35}P one.*

From spherical to deformed nuclei

For closed-shell nuclei, nucleons occupy all possible magnetic sub-states, leading to a globally spherical spatial repartition of the nucleons (see left sketch of Figure 12). As we saw earlier, this is no longer true in open shells, in which slightly deformed shapes are present. When spherical shell gaps are weakened significantly enough, cross shell excitations can develop and become more favoured than the inert configurations. In such cases, the nucleons have many more configurations as compared to the ones provided with a single shell. It follows that when several orbits come into play, nucleons can maximize their quadrupole energy by occupying all possible configurations in each orbit having a

maximum overlap with a spheroid shape, as schematically shown in the right sketch in the left hand side of the Figure 12. This holds as orbits come closer in energy, where one can no longer make a sharp separation between an inert core and valence orbits. There, nucleons from two different shells mix and maximize their quadrupole energy to give rise to deformed structures. These nuclei often exhibit rotational spectra with energy scaling in $\hbar^2 J(J+1)/2\Im$, with a moment of inertia $\Im$ greater for larger deformation, as for the rigid rotor in classical mechanics. At larger deformation, the first excited state 2^+ is significantly lowered. This 2^+ energy value is the first experimental hint for the presence of deformation in nuclei. In parallel, the probability to excite this state B(E2) is increased, as many nucleons are involved coherently to give this configuration (also called collective mode).

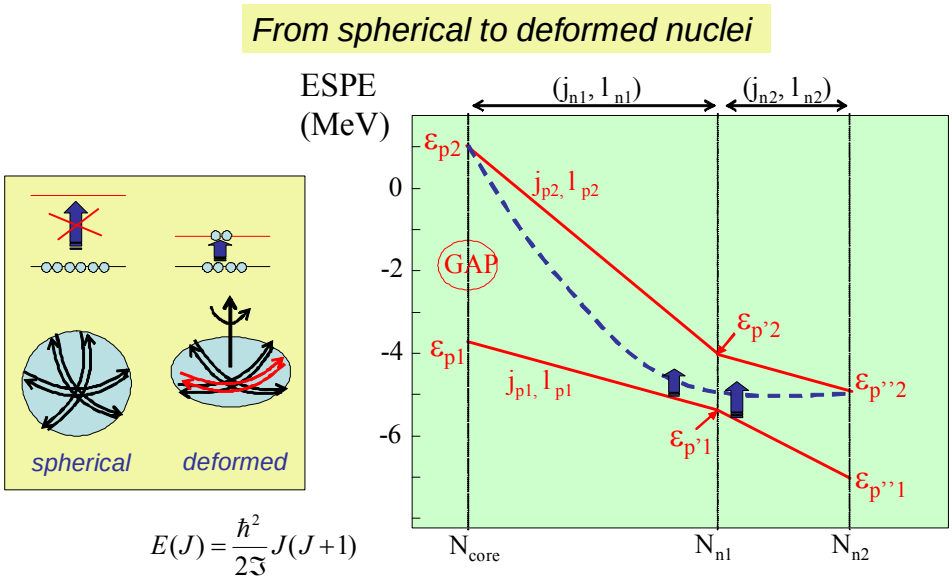

Figure 12: ***Left*** *: Schematic view of sub-states configurations in the case of a closed shell which cover a sphere. When a shell gap weakens, nucleons can occupy the state located immediately above and adopt sub-states in a given direction leading to a deformed configuration.* ***Right*** *: Schematic view of a shell gap reduction, due to excitations from the core to valence states.*

We have now presented all concepts and definitions that are pre-requisites to look at shell evolution, from spherical to deformed configurations. Before moving to the next parts dealing with detailed studies of the evolution of the N=20 and N=28 gaps, let us remind the key messages of this part on nuclear interaction and shell evolution.

Take away message: Part II

Key information derived on the nuclear in-medium interactions and evolution of shell gaps

- Proton-neutron interactions are largest when the two nucleons occupy orbits with the same n, ℓ and opposite total angular momenta j> and j< (e.g. $f_{7/2}$ and $f_{5/2}$ in which ℓ =3). For interaction between like-nucleons, the pairing energy makes the NN interaction more bound between j> and j> nucleons (e.g. $g_{9/2}$ and $g_{9/2}$ for ℓ =4)

- Monopole energies correspond to the 'effective' or 'in-medium' mean nuclear energy, averaged over all directions of the two nucleons in interaction

- The slope of Effective Single Particle Energies (ESPE) of the orbits as a function of an increasing nucleon number is given by the monopole energy

- Shell gaps are given by differences between adjacent ESPE. They vary when the monopole terms involved are significantly different

- Monopole intensities are largest for light nuclei, and decrease in strength as the nucleus grows in size. Consequently shell evolutions are sharper in light nuclei

- Experimental binding energy often exceeds the ESPE value by the gain of correlation energy (quadrupole, pairing…). They are the closest to ESPE for nuclei around shell closures

PART III: THE N=20 SHELL CLOSURE

Introduction

The first indications of a vanishing of a shell closure in the chart of nuclides were revealed around the neutron magic number N=20. It was found that ^{31}Na (Z=11) and ^{32}Mg (Z=12) exhibit anomalies in their binding energies [Thib75], mean-square charge radii [Hube78] and nuclear spectra [Detr79,Guil84]. The extra binding energy of these nuclei, with respect to their neighbours, was attributed to their deformation which was quickly associated with particle-hole excitations across the N=20 shell [N20]. The spherical N=20 gap is thus not large enough to prevent excitations and correlations to develop to the fp shells in the $_{12}$Mg isotopic chain. As these fp orbits lie outside the normal model space description of the sd shells, they are often referred to as *intruder states*. For some nuclei, the intruder and normal configurations are inverted in energy. They belong to the so-called "*Island of Inversion*" [Warb90]. Soon after this finding many experimental and theoretical efforts have been devoted to determine the boundaries of this Island, and to understand the underlying physics driving this sudden change between pure sd and full sdfp configurations. The gain of binding energy through deformation was also invoked to explain why the drip line extends further in the F and Ne than in the O isotopic chain.

Thanks to the advent of radioactive ion-beam facilities worldwide, the evolution of the N=20 shell closure and the appearance of a new magic number at N=16 far from the valley of stability are now well established and much better understood. In the following chapters we will use different experimental information to investigate the evolution of the N=20 shell gap, using the systematic of the binding energies, trends in 2^+ energies and reduced transition probabilities B(E2; $0^+ \rightarrow 2^+$), transfer and knock-out reactions. Finally the underlying physics parameters which reduce the size of the N=20 gap and increase the N=16 one will be discussed.

Predicted shell evolution at N=20

For sake of pedagogy, we start this session on the evolution of the N=20 shell closure by theoretical predictions, which will then be confronted to experimental results. It should however be mentioned that often experimental results have preceded or greatly influenced the theories. One should therefore have in mind that theory and experiment benefit from each others works.
Figure 13 shows variations of neutron ESPE for the N=20 isotones, which correspond to the monopole-driven changes in energy. These predictions [Utsu99] are based on experimental constraints, which will be described in the following. Globally, one sees that the neutron ESPE have the same slopes, due to the fact that most of the proton-neutron interactions have similar intensities. This remark does not hold for the $d_{5/2}d_{3/2}$ interaction which is predicted to be significantly larger, as for this interaction protons and neutrons have the same angular momentum and opposite spin directions. It follows that the N=20 shell gap is constant between Ca (Z=20) and Si (Z=14), and abruptly decreases below Z=14 when the proton $d_{5/2}$ orbit is getting emptied. The removal of all $d_{5/2}$ protons makes the neutron $d_{3/2}$ orbit likely to be unbound in the Z=8 ^{28}O nucleus. Added to this disappearance of the N=20 gap, a new magic number is predicted to exist at N=16 in the O isotopes.
The decrease of the N=20 gap enables cross shell excitations to develop between the occupied sd shells and the valence fp ones. This leads to a gain of quadrupole collectivity due to the fact that the N=20 shell is no longer closed. This increase of cross shell excitations should be associated with enhanced occupancy of the fp states in the ground state wave function of ^{32}Mg (Z=12). All these four points (i) particle instability of ^{28}O, (ii) disappearance of the N=20 gap below ^{34}Si, (iii) enhancement

of fp orbits occupancy in ^{32}Mg, (iv) emergence of a new N=16 gap below Z=14, will be examined in the following chapters.

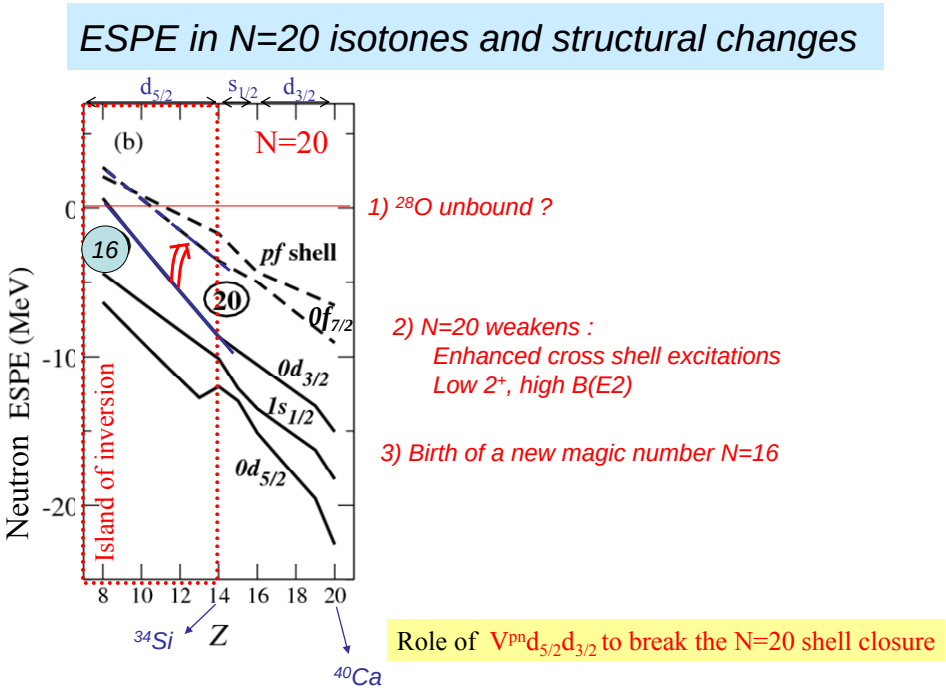

Figure 13: Calculated neutron effective single particle energies (ESPE) of the $d_{5/2}$, $s_{1/2}$, $d_{3/2}$, $f_{7/2}$ and $p_{3/2}$ orbits for the N=20 isotones as a function of proton number Z [Utsu99]. While increasing the proton number, several proton orbits $d_{5/2}$ (Z=8-14), $s_{1/2}$ (Z=14-16) and $d_{3/2}$ (Z=16-20) are progressively filled. In particular it is predicted that the filling of the proton $d_{5/2}$ orbit leads to the formation of the N=20 gap, as well as the disappearance of the N=16 one. When approaching the valley of stability (Z>14) the size of the N=20 gap remains large and constant, about 6MeV.

Search for particle stability of ^{28}O.

The search for particle stability of ^{28}O, which is composed of the two magic numbers Z=8 and N=20, was carried out worldwide [GANIL, Nota02, NSCL]. We show in Figure 14 an example of the nuclei produced by the fragmentation of an ^{40}Ar beam to produce nuclei in the vicinity of ^{28}O [Nota02]. Fragments were selected by a spectrometer to transmit the nuclei of interest. They are identified in Z and A/Z, the groups of black points corresponding to the various nuclei produced. Despite many efforts, it was finally deduced that ^{28}O (which should lie inside de blue circled area at A/Z=3.5) is unbound with respect to neutron emission(s). This feature may arise from the fact that the neutron $d_{3/2}$ orbit is unbound. Note that the last bound O isotope is ^{24}O, while ^{25}O which contains one neutron in the $d_{3/2}$ orbit is unbound by about 770 keV [Hoff08][6].

[6] Using the attractive neutron-neutron monopole $V^{nn}d_{3/2}d_{3/2}$ ~ - 400keV derived in the valley of stability, the ^{28}O should be bound. Its particle instability calls for a modification of the nuclear interactions for weakly bound systems. Some theoretical attempts are being carried out to explore the role of pairing, three body repulsive forces and coupling to continuum to account for the observed limit of particle-stability boundary in this region of the chart of nuclides.

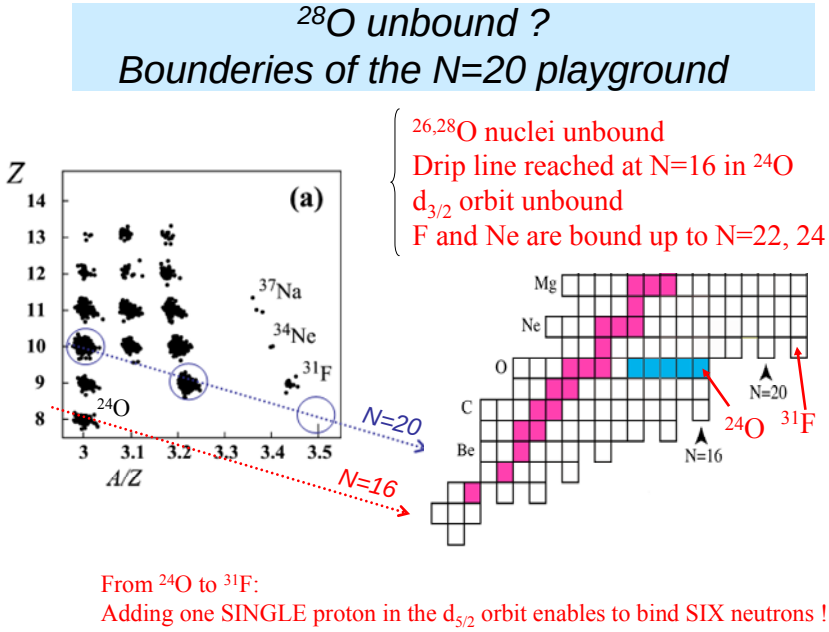

Figure 14: Particle identification in Z and A/Q of the nuclei produced through the fragmentation of a ^{40}Ar beam at RIKEN [Nota02]. It is seen that while the drip line extents up to N=22 in the F chain, the last bound O nucleus is ^{24}O, which contains only 16 neutrons.

As soon as one proton is added in the $d_{5/2}$ orbit (leading to the $_9$F chain), up to six neutrons can be added to keep the $^{31}F_{22}$ nucleus bound. This shows the strength of the proton-neutron interaction $V^{pn}d_{5/2}d_{3/2}$ to bind the $d_{3/2}$ neutron orbit by adding four neutrons to reach ^{29}F. Other explanation should be invoked to bind two more neutrons to reach ^{31}F. There the fp shells start to be filled. The breakdown of the N=20 shell closure could encourage excitations across N=20, leading to a gain of correlations. The very neutron-rich ^{31}F would therefore be deformed. This is to be checked in a far future. One notices also in Figure 14 that the odd neutron nuclei are often unbound (e.g. ^{28}F, ^{30}F), while the even neutron ones (^{29}F, ^{31}F) are bound. This odd-even effect is due to pairing interaction which favours the particle stability of nuclei having paired neutrons.

Disappearance of the N=20 magic number

Figure 15 shows the evolution of the neutron N=20 shell closure, south to ^{40}Ca, though three parameters, (i) the 2 neutron separation energies S_{2n} (ii) the evolution of 2^+_1 energies and (iii) the reduced transition probability B(E2: $0^+_1 \rightarrow 2^+_1$). The S_{2n} curve exhibits a sharp drop in the Ca isotopic chain, after having passed the N=20 shell gap. This is explained by the fact that, while adding 2 extra neutrons above the gap, it becomes suddenly easier to take them out of the potential well. This drop of S_{2n} is a typical feature of the passage through a shell gap. While looking at the Mg chain, this drop is no longer observed. Rather the S_{2n} looks greater at N=22 than at N=20. This points to the disappearance or at least the weakening of the N=20 shell gap. As discussed earlier, this gain of binding energy at N=20 is well accounted for by the increase of correlations (or deformation).

Another typical feature of magic nuclei is that they exhibit higher excitation energies (here 2^+_1 states), due to the fact that the promotion of nucleons to the upper shell (across the large gap) requires significant energy. This rise in energy at N=20 holds remarkably well for ^{40}Ca, ^{36}S (Z=16), and ^{34}Si (Z=14), but fails dramatically again at Z=12 where the 2^+ energy decreases instead[7].

[7] Note that on the one hand for the Ca, S and Si and on the other hand for the Mg isotopic chain, the 2^+_1 state does not have the same origin. It comes mainly from neutrons excitations for the first group (for which Z=20, 16 and 14 are strong shell or sub-shell closures) and from proton and neutron excitations for Mg. This explains why the 2^+ energies are globally weaker in Mg. However the breakdown of the neutron N=20 shell gap accounts for the decrease of the 2^+ at N=20.

Last observable is the probability B(E2) to excite these 2^+ states. For closed shell nuclei, this value is relatively weak as few nucleons contribute to it. It is remarkably constant in ^{38}Ar, ^{36}S and ^{34}Si, but increases by a factor of 4 in ^{32}Mg [BE2mg32] demonstrating that many nucleons participate collectively to this excitation. The B(E2) value for ^{30}Ne remains to be determined… Shell model calculations which take this weakening of the shell closure into account (denoted as 'no gap' in Figure 15) better reproduce the experimental data.

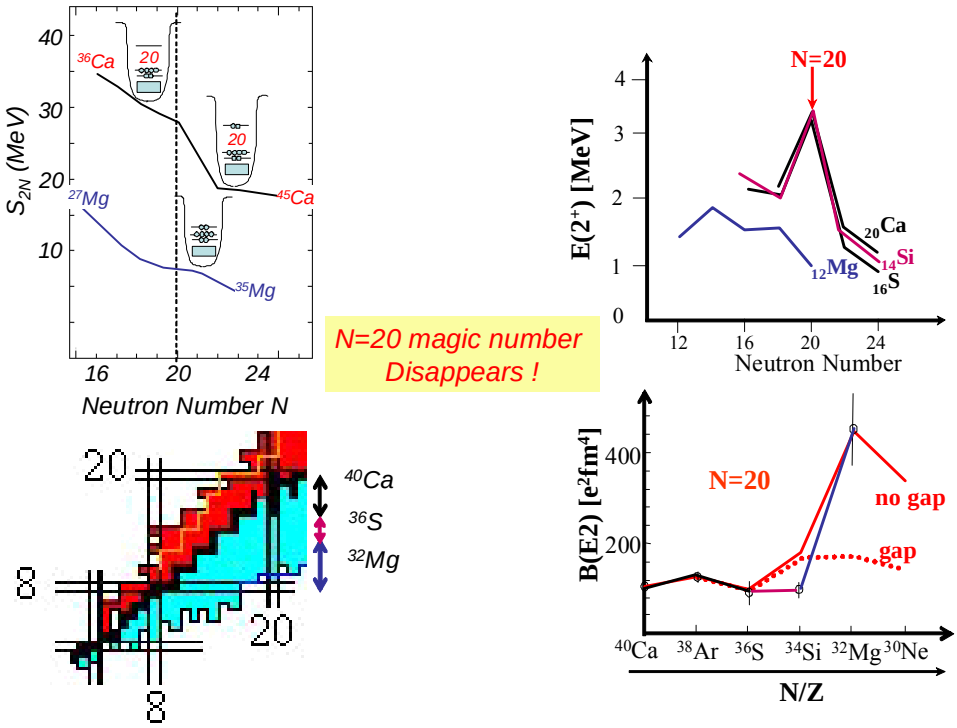

Figure 15: ***Top left*** *: Systematic of two neutron separation energies S_{2n} in the Ca and Mg isotopic chains.* ***Top right****: Systematic of first 2^+ energies in the Ca, S, Si and Mg isotopic chains.* ***Bottom right*** *: Systematic of B(E2) values in the N=20 isotones. Shell model calculations [Moto95] assuming a breakdown of the N=20 gap (full line denoted as 'no gap') or a strong shell closure (dotted line denoted as 'gap') are compared to the data. Gathering all these pieces of information, it is found that the N=20 shell closure should be substantially eroded when protons are removed from the $d_{5/2}$ orbit.*

To summarize, the N=20 shell gap remains present while removing protons from the $d_{3/2}$ and $s_{1/2}$ orbits (from Z=20 to Z=14), but collapses when protons start to be removed from the $d_{5/2}$ orbit (Z=12). One should notice that the removal of protons from the $d_{3/2}$ or $d_{5/2}$ orbits give rise to very different structural consequences. The former leaves the N=20 gap constant, while the second strongly modifies it. Between the $d_{3/2}$ and $d_{5/2}$ orbits, the major change is the spin orientation of the protons with respect to their angular momentum. Therefore this points to a strong dependence of nuclear forces with spin orientations, such as spin-orbit and tensor forces.

Occupancy of the intruder fp states in ^{32}Mg

Another consequence of a reduced shell gap is the subsequent increase of cross-shell excitations which leads to the partial occupancy of the upper fp 'intruder' states. The occupancy of the in principle vacant fp states can be determined by using neutron knock-out reactions from the ^{32}Mg nucleus [Terr08]. This occupancy is to be compared to the neighbour nucleus ^{30}Mg. It is shown from knock-out reactions using ^{30}Mg and ^{32}Mg beams that the fp occupancy moves from 0.5 (first row of the right hand side of Figure 16) to about 2 in ^{32}Mg (right row). If the N=20 shall gap was large, the normal occupancy of these fp shells should be zero. In the case of ^{32}Mg a mean value of 2 neutrons occupy in average the fp states, which calls for a 2 particle excitations, leaving two holes below in the sd shells. This excitation is often called a 2p2h excitation. For this nucleus, this 2p2h configuration becomes

more bound than the one in which all neutrons reside in the sd shell. An inversion between the normal (fully occupied sd) and intruder (partial fp occupancy) configuration has occurred. Therefore, it is often said that ^{32}Mg belongs to an island of inversion.

Large occupancy of fp shells at N=20 ! 2p2h mechanism

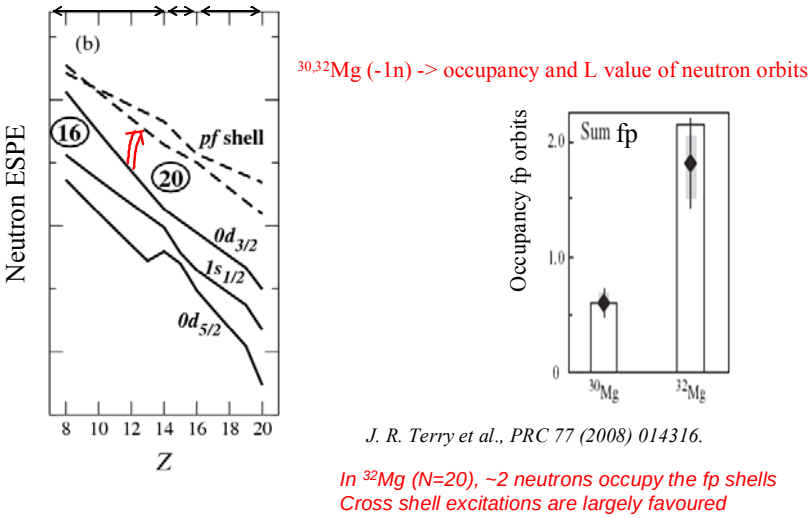

Figure 16: The occupancy of the fp orbits has been derived from one neutron knock-out experiments at MSU/NSCL using beams of ^{30}Mg and ^{32}Mg [Terr08]. It is shown that the fp occupancy grows from about 0.5 to 2 between these two Mg isotopes. This indicates the increasing porosity of the N=20 gap, and reveals that excitations of 2 particles – 2 holes are preferred over the closed $d_{3/2}$ shell configuration.

A new magic number N=16

The fourth expected consequence of this strong proton-neutron interaction is the birth of a new magic number N=16 for Z~8. To investigate this, the transfer reaction ^{22}O(d,p)^{23}O reaction was used in reverse kinematics using a secondary beam of ^{22}O produced at the RIKEN facility [Elek07]. The beam was tracked by position-sensitive gas-filled detectors to a CD_2 target (containing deuterons) in which the ^{22}O nuclei can interact. In the selected (d,p) reaction a neutron is 'deposited' in the valence orbits, which can be bound or unbound with respect to neutron emission. The proton energies and angles are determined to infer the energy of the neutron orbits in ^{23}O. The angular distribution of the protons can be used to determine the transferred momentum during the reaction, leading to a ℓ assignment of the state in which the neutron was deposited. Emitted protons from the (d,p) reaction were detected in a large array of CSI detectors. In addition a neutron wall was placed at the most forward angles to detect transfer reactions to neutron unbound states. In such cases, a proton and a neutron are emitted. The schematic experimental set-up is shown in Figure 17.

Search for a new magic number N=16 :

Use of $^{22}O(d,p)^{23}O$ to probe the neutron N=16, 20 shell closures

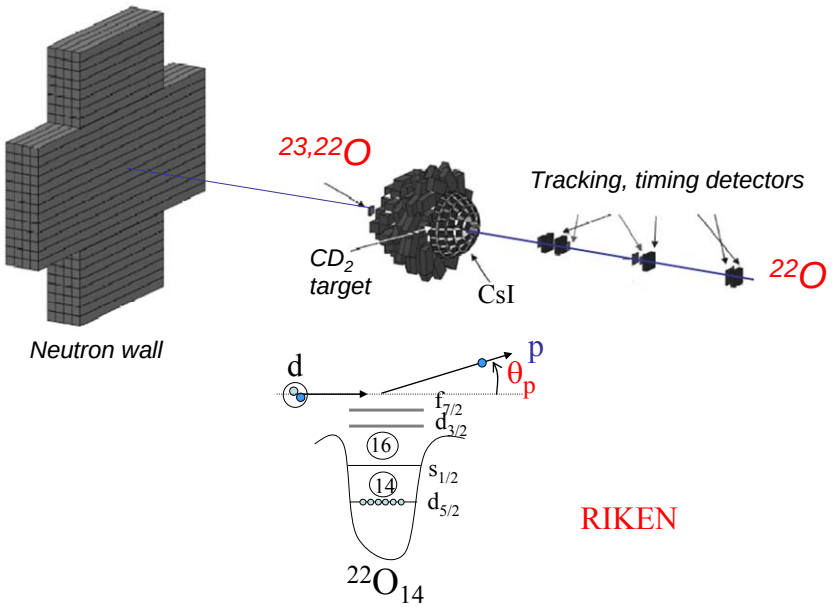

Figure 17: Schematic view of the $^{22}O(d,p)^{23}O$ set up, with the tracking detectors, the target surrounded by a large array of CsI detectors. In the forward direction a wall of neutron detectors is used to infer whether the transfer has occurred to unbound states in ^{23}O, as shown for the $d_{3/2}$ in the bottom part of the figure [Elek07].

The 'sizes' of the N=20 and N=16 gaps in Oxygen

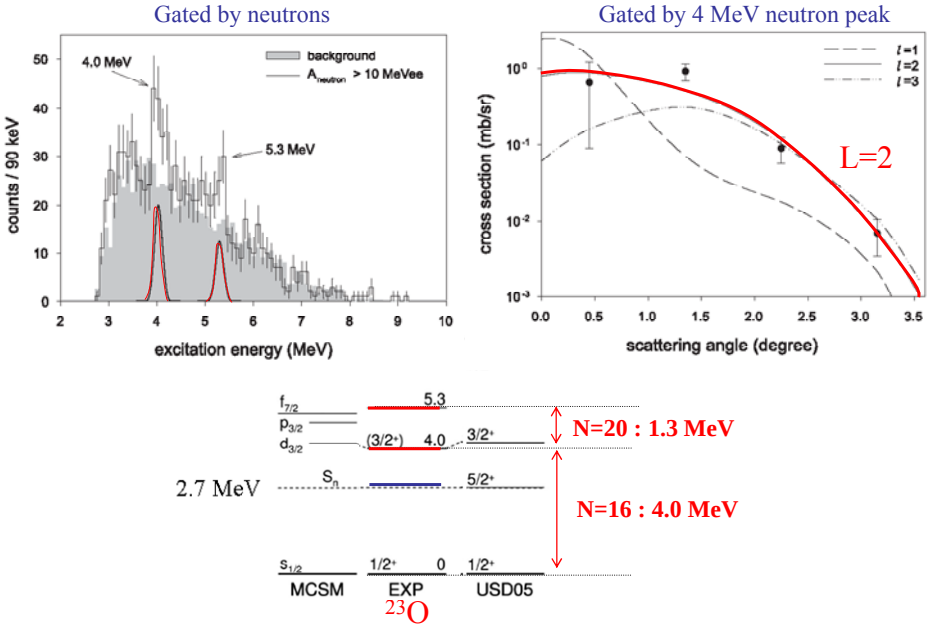

*Figure18: **Top** : **Left** Excitation energy spectrum in ^{23}O obtained from the protons collected during the (d,p) reaction in coincidence with neutrons. **Right** Angular distribution of the protons gated by the 4 MeV peak. Experimental data points are compared to DWBA model calculations assuming ℓ=1-3 angular momentum. The ℓ=2 value gives the best fit, leading to a tentative $d_{3/2}$ assignment for this state. **Bottom** : Experimental results of Elekes et al.[Elek07] (in red) and of Schiller et al. [Schi07] (in blue) are compared to Monte Carlo Shell Model (MCSM) or USD05 calculations which takes the full sdfp valence space into account or which is restricted to the sd shells, respectively. The sizes of the N=16 and N=20 shell gap are inferred to be of about 4MeV and 1.2MeV, respectively.*

The neutron-gated proton spectrum, obtained from the (d,p) transfer reaction, is shown in the top left hand side of Figure 18. Two peaks are seen at 4 and 5.3 MeV excitation energies in the ^{23}O nucleus. They both correspond to transfer to unbound states, as ^{23}O is bound by only 2.7 MeV. For the first peak, an angular distribution has been obtained, favouring an ℓ=2 assignment for the populated valence state. This is likely to correspond to the transfer of a neutron into the unbound and unoccupied $d_{3/2}$ orbit. Guided by Monte Carlo Shell Model (MCSM) calculations [Utsu99], the other peak probably corresponds to one of the fp orbits. Even is the statistics is weak in the present experiment, we can surmise two important features:

-The high energy of the $d_{3/2}$ state confirms the emergence of a new magic number N=16 between $s_{1/2}$ and $d_{3/2}$ orbit, with an energy gap of about 4 MeV, as shown in the bottom part of Figure 18.

-The other state at 5.3 MeV, considered to be an intruder state would lead to a N=20 shell gap in ^{23}O as small as 1.3 MeV. If confirmed with larger statistics it would prove the disappearance of the N=20 shell gap in the O isotopes. Note that these statements hold true if this state carries a large spectroscopic factor value.

We note that for these nuclei, the N=28 gap between the $f_{7/2}$ and $p_{3/2}$ orbits is also predicted to be very weak and the ordering between the f and p states is expected to be reversed (see Figure 13 and 18 bottom). This is at variance with a large N=28 gap of about 4.9 MeV in ^{48}Ca or 2 MeV in ^{40}Ca between the $f_{7/2}$ and neutron $p_{3/2}$ orbits. This reduction of the N=28 gap when protons are removed from the $d_{5/2}$ orbit can be ascribed to the corresponding monopole terms involved. Indeed the N=28 gap will be changed according to the monopole energy difference ($V^{pn}(d_{5/2}p_{3/2})$ - $V^{pn}(d_{5/2}f_{7/2})$). The reduction of N=28 then follows from the fact that in absolute value $V^{pn}(d_{5/2}p_{3/2}) < V^{pn}(d_{5/2}f_{7/2})$. I invite the reader to qualitatively understand why it is so using the properties on the nuclear force mentioned in Part II.

General evolution of HO-like magic numbers: the role of nuclear forces

To summarize, we have seen that while the N=20 is large in the valley of stability between ^{40}Ca and ^{36}S, it disappears quickly below ^{34}Si due to the fact that the $V^{pn}d_{5/2}d_{3/2}$ (spin-flip) monopole interaction is the largest among all others in the sd valence space. A noticeable consequence is the emergence of a new magic number N=16 which has been proven experimentally. Interesting is to see whether this spin-flip interaction is playing a similar role in other parts of the chart of the nuclides. While the $V^{pn}d_{5/2}d_{3/2}$ interaction corresponds to ℓ=2, the corresponding interactions with ℓ=1 and ℓ=3 would be $V^{pn}p_{3/2}p_{1/2}$ and $V^{pn}f_{7/2}f_{5/2}$, respectively.

Figure 19 shows schematically that a reduction of the associated N=8, 20, and 40 harmonic oscillator shell gaps is indeed observed when the proton $p_{3/2}$, $d_{5/2}$ and $f_{7/2}$ orbits are no longer filled, respectively. For the former gap the removal of $p_{3/2}$ protons leads to a much smaller binding energy of the neutron $p_{1/2}$, which comes closer to the sd intruder states. This mechanism has a profound impact on the appearance of halo states in ^{11}Be, in which the intruder $s_{1/2}$ orbit becomes the ground state. For the latter, the removal of $f_{7/2}$ protons from Ni provokes the destruction of the N=40 HO shell gap as the $f_{5/2}$ neutron orbit comes close to the upper $g_{9/2}$ orbit. More generally all these cases correspond to more neutron-rich nuclei, in which the magic numbers 8, 20 and 40 no longer exist. As a by product of this process, new sub-shell gaps are created at N=6, 16, and possibly 34. This beautiful analogy between these three HO shell closures is also visible in the 2^+_1 energy systematics.

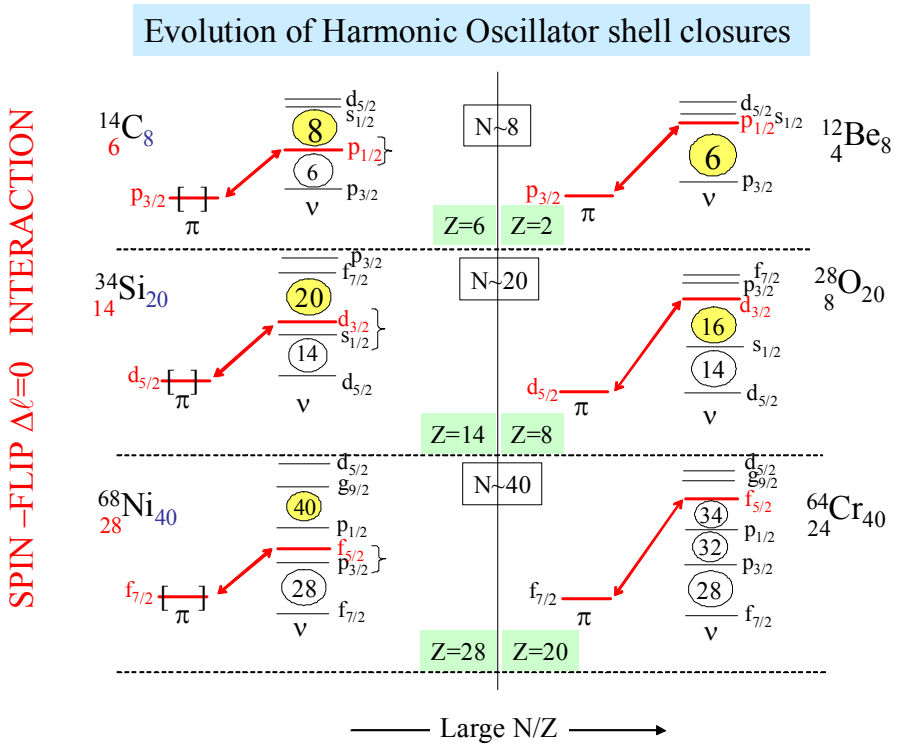

Figure 19: Schematic evolution of N=8, N=20 and N=40 HO shell gaps as a function of the filling of the proton $p_{3/2}$, $d_{5/2}$ and $f_{7/2}$ orbits, respectively. One sees that the spin-flip interaction between the proton and neutron spin-orbit partners changes dramatically the energy of the neutron $p_{1/2}$, $d_{3/2}$, and $f_{5/2}$ orbits.

As shown in Figure 20, a very similar pattern is found when comparing the evolution of 2^+_1 energies in the N=8, N=20 and N=40 isotones. A quick structural change is found between $_6$C and $_4$Be at N=8, $_{14}$Si and $_{12}$Mg at N=20, and $_{28}$Ni and $_{26}$Fe at N=40. Interesting is the fact that the $_{24}$Cr are the highly deformed nuclei around N=40. They are located at mid $f_{7/2}$ proton shell. Discussions related to the island of inversion in the N=8 and N=40 nuclei can be found in Refs. [N8] and [N40], respectively.

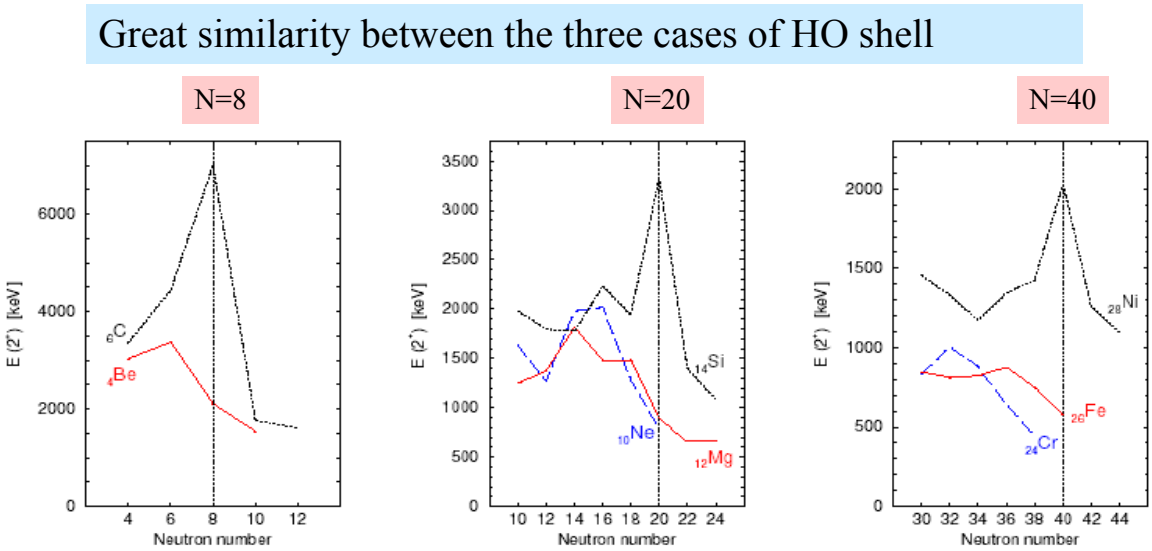

Figure 20: Systematic of 2^+_1 energies for the N=8, N=20 and N=40 isotones. For the most neutron-rich nuclei the rise in 2^+ energies, which characterizes a shell closure, is no longer observed.

PART IV: THE SPIN-ORBIT MAGIC NUMBER N=28

Introduction

The magic number N=28, revealed for instance in ^{48}Ca, is formed by the combined action of the one-body spin-orbit (SO) interaction and by the neutron-neutron interactions. The former part is rather well known. As shown in Figure 4, the SO interaction lowers the $f_{7/2}$ neutron orbit in the middle of the sd and fp oscillator shells, resulting in a shell gap between the $f_{7/2}$ and $p_{3/2}$ orbits. The second effect, which is rarely evoked, accounts for the increase of this gap by as much as 3 MeV between ^{40}Ca to ^{48}Ca while eight neutrons are added into the $f_{7/2}$ orbit. This is due to the fact that the neutron-neutron monopole $V^{nn}f_{7/2}f_{7/2}$ is attractive (about -0.23 MeV), while the $V^{nn}f_{7/2}p_{3/2}$ is repulsive (about +0.16 MeV). This can be viewed in left hand side of Figure 21 where the binding energies of the $f_{7/2}$ ($p_{3/2}$) are moving downward (upward). This effect is taken into account in shell model descriptions of the nucleus, which use experimental binding energies as constraints. However, this increase of the size of the N=28 shell gap due to neutron-neutron interactions is not considered in mean field approaches such as the simple Woods Saxon potential, or as in the more evolved Hartree-Fock approach using the Gogny force. As a result, the size of the N=28 remains constant in these two mean-field theories.

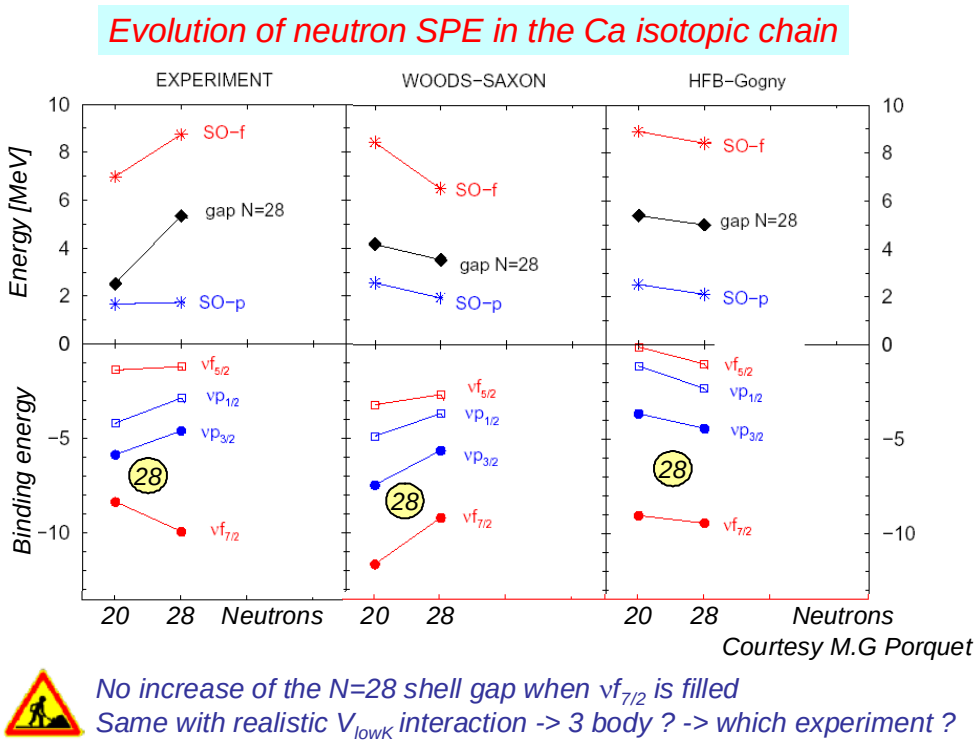

Figure 21: Experimental (Left part) and calculated (central and right part) evolutions of the binding energies of the neutron $f_{7/2}$, $p_{3/2}$, $p_{1/2}$ and $f_{5/2}$ orbits as a function of the filling of the neutron $f_{7/2}$ orbit from N=20 to N=28. The upper part of the Figures shows differences in binding energies, such as the N=28 gap (between $f_{7/2}$ and $p_{3/2}$) or the spin-orbit splittings ($f_{7/2}$ - $f_{5/2}$ or $p_{3/2}$ - $p_{1/2}$). This Figure [Porq09] shows that the two mean-field models (Woods Saxon and Hartree Fock with the Gogny force) do not reproduce the experimental increase of the N=28 gap, and cannot account for the correct evolution of the SO splitting between the f orbits.

On the other hand the N=28 gap is well accounted for by phenomenological (or empirical) two-body interactions as they are fitted to the available data. Figure 22 shows the results of two commonly used shell model interactions GXPF1 and KB3G. Conversely it is interesting to see that this increase of

shell gap cannot be reproduced using two-body realistic forces, such as the low momentum V_{lowK}[8] one extracted from bare NN interactions and 'dressed' to take into account the finite size of a nucleus and the occupancy of the shells. Rather, it is shown that three body forces are required to better account for creating the N=28 shell gap. The reader may wonder why the *two-body* interactions GXPF1 [GXPF1] and KB3G [KB3G] can account for the correct experimental trend, while *three-body* forces are required when realistic forces are used [Schw10]. This comes from the fact that empirical two body interactions intrinsically contain three body effects.

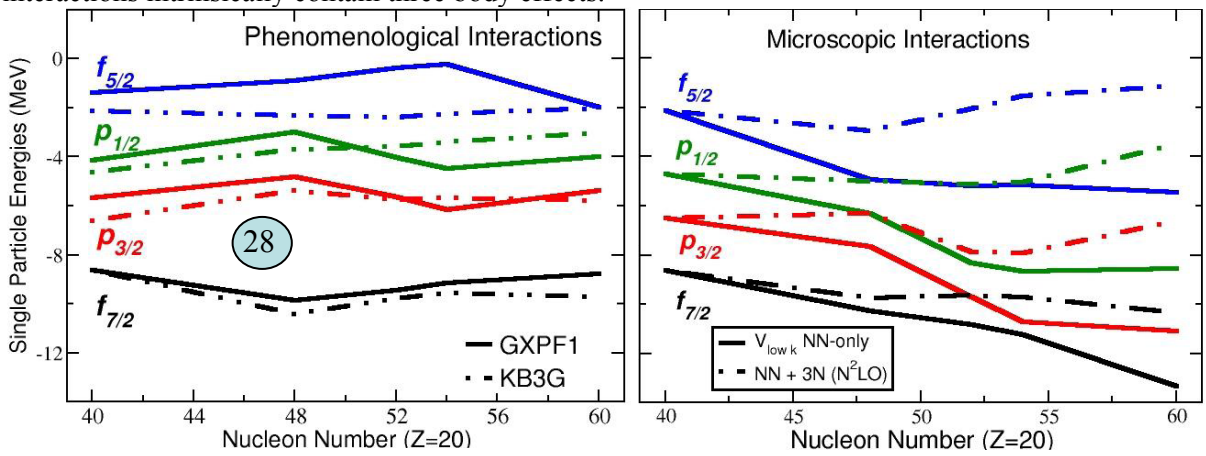

Figure 22: ***Left****: Effective neutron single particle energies obtained in the Ca isotopic chain for the fp shells using the GXPF1[GXPF1] and KB3G [KB3G] phenomenological two-body interactions. As these interactions are constrained by experiments data, they give almost similar results when information exists, while they diverge otherwise, e.g. at large neutron numbers.* ***Right****: Same plot using the so called V_{lowK} interaction [VlowK] (full line) derived from free NN interactions and by adding three body forces (dashed dotted line). One sees that the N=28 gap cannot be reproduced using realistic interactions only when three body forces are taken into account [Schw10].*

Even if the absolute values of the neutron-neutron monopoles (or the T=1 term) is relatively small as compared to neutron-proton values (about 1/3), the attractive $V^{nn}f_{7/2}f_{7/2}$ monopole plays an essential role here to create the N=28 shell gap. The same mechanism is at play to create all spin-orbit shell gaps, such as N=14 and N=50, in which the $V^{nn}d_{5/2}d_{5/2}$ and $V^{nn}g_{9/2}g_{9/2}$ attractive monopoles are involved, respectively.

Evolution of the N=28 shell closure driven by proton-neutron interactions

The playground for studying the N=28 shell evolution is sketched in Figure 23: in ^{48}Ca the protons fully occupy the $d_{5/2}$, $d_{3/2}$ and $s_{1/2}$ orbits. While moving from ^{48}Ca to ^{42}Si, protons are progressively removed from the two orbits $s_{1/2}$ and $d_{3/2}$, which are degenerate in energy as shown in Figure 10. The $d_{5/2}$ proton orbit remains a priori filled. While going to ^{42}Si, protons are therefore removed equiprobably from the $d_{3/2}$ and $s_{1/2}$ orbits. It follows that the neutron orbits can be modified by this change of involved proton-neutron interactions. Therefore the evolution of single particle energies gives key information on the action of nuclear forces, such as the tensor force between the $d_{3/2}$ protons and the $f_{7/2}$ or $f_{5/2}$ neutrons. The effect of these forces can eventually modify the N=28 gap, and change the size of the neutron SO p and f splittings. From the point of view of the proton orbits, nuclear forces act to reduce the size of the proton Z=14 gap between the stable ^{36}S and the N=28 ^{44}S nucleus (see Figure 11). If both the Z=14 and N=28 gap were reduced, cross-shell excitations would develop between the normally occupied and the valence orbits. As occupied and valence states are separated by 2 units of angular momenta ($\Delta\ell$=2), quadrupole excitations are the most likely to develop. In the following chapters we shall look at the evolution of neutron single particle orbits and at the onset of deformation while removing $s_{1/2}$ and $d_{3/2}$ protons.

[8] V_{lowK} corresponds to the low momentum part of realistic forces, which is sufficient to describe the spectroscopy of nuclei. Hard core repulsion gives rise to much larger momentum values *k* which are not required here.

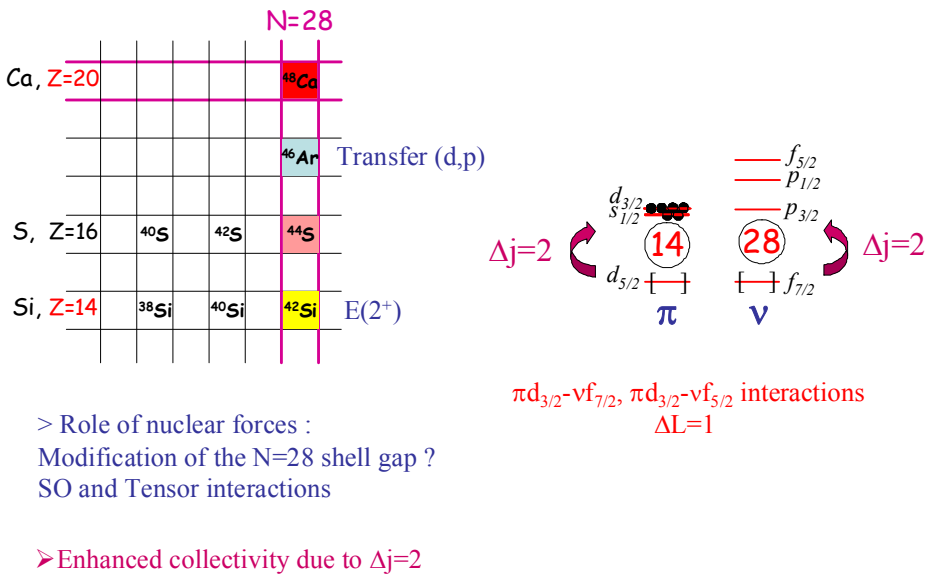

Figure 23: Schematic view of the orbits involved in the proton sd and neutron fp shells. The mechanism for increased E2 excitations across the proton and neutron shells is also exemplified.

As shown schematically in the upper left part of Figure 24, the transfer reaction ^{46}Ar(d,p)^{47}Ar enables to probe the energy and vacancy of neutron unoccupied p or f states in ^{46}Ar [Gaud06]. In this process a neutron is deposited in the ^{46}Ar nucleus, leaving a free proton which was detected in the highly segmented Si detector array (MUST). As ^{46}Ar is unstable, this experiment has been done in reverse kinematics using an ^{46}Ar beam provided by the SPIRAL/GANIL facility. Using the proper kinematics rules, the energy of the protons (which scales according to the binding energy of the neutron orbit to which the neutron was deposited) can be converted in the excitation energy in ^{47}Ar.

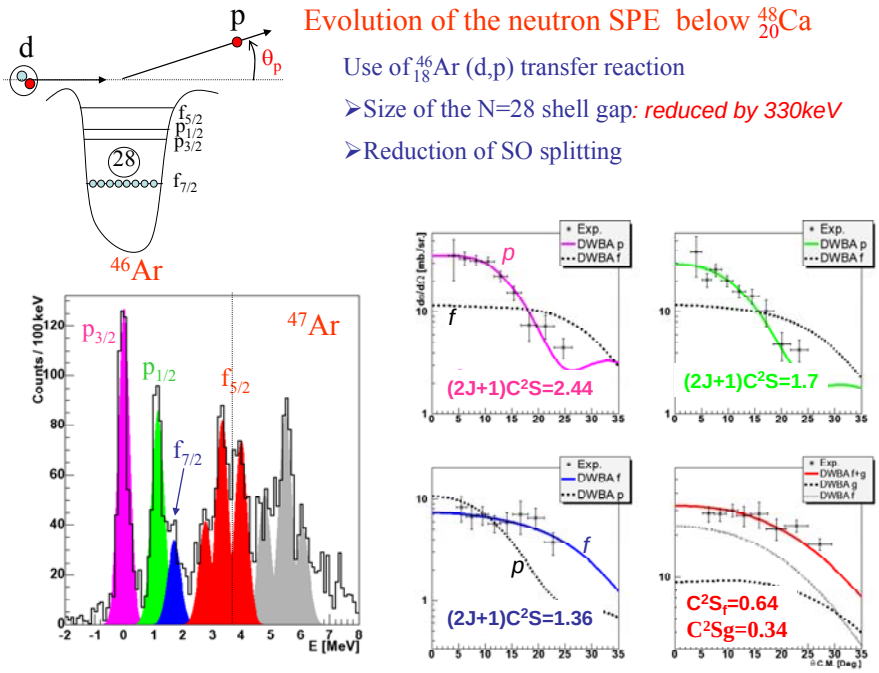

*Figure 24: **Top**: Sketch of the (d,p) transfer reaction in neutrons are deposited in one of the empty fp shells. **Bottom Left**: Excitation energy spectrum of ^{47}Ar produced by the (d,p) transfer reaction. **Bottom right**: Proton angular distributions gated by the coloured peaks in the excitation energy spectrum. Comparison to DWBA calculations is used to assign ℓ values to the states [Gaud06].*

Transfer to the $p_{3/2}$ state occurs at the reaction Q value (here S_n), which exactly corresponds to the size of the N=28 gap, if the $f_{7/2}$ and $p_{3/2}$ ground state are purely single particle states. One sees a clear peak at zero excitation energy in the bottom left of Figure 24 which corresponds to this transfer channel. The corresponding proton angular distribution is shown in the right part of Figure 24. Comparison of the angular distribution to DWBA calculations shows that the two first states have ℓ=1 (p states). The normalization of the experimental data (shown with crosses) to the calculation gives the value of the spectroscopic factor C^2S, or (2J+1) C^2S which is the vacancy value of the state. Error bars of about 20% should be considered. They mainly arise from the imprecision due to the treatment of the reaction mechanism by optical potentials. For a strictly closed-shell nucleus, the vacancy of the 'normally' occupied states is 0, while the value for valence states is (2J+1), which is the maximum number of neutrons the orbit can contain. For instance the $p_{3/2}$ vacancy should be a priori equal to 4, while the expected $f_{7/2}$ vacancy would be 0. Deviation to the maximum vacancy value (2.44 instead of 4) indicates that the $p_{3/2}$ was already partly occupied by about 1.5 neutrons (4-2.44) in ^{46}Ar. Interesting is to see that a partial vacancy of the $f_{7/2}$ shell of 1.36 is seen. This value approximately corresponds to the missing strength of the $p_{3/2}$ orbit. This indicates that in ^{46}Ar, some particle-hole excitation already occur between the normally occupied $f_{7/2}$ and valence $p_{3/2}$ neutron orbits, indicating some porosity of the N=28 shell gap. Transfer to the other $p_{1/2}$ and $f_{5/2}$ orbits are also identified, completing the panel of states that can be fed by the (d,p) reaction. None of the observed state is of pure single particle character, as they are all more or less coupled to the 2^+ excitation of the core[9], located at about 1.5 MeV.

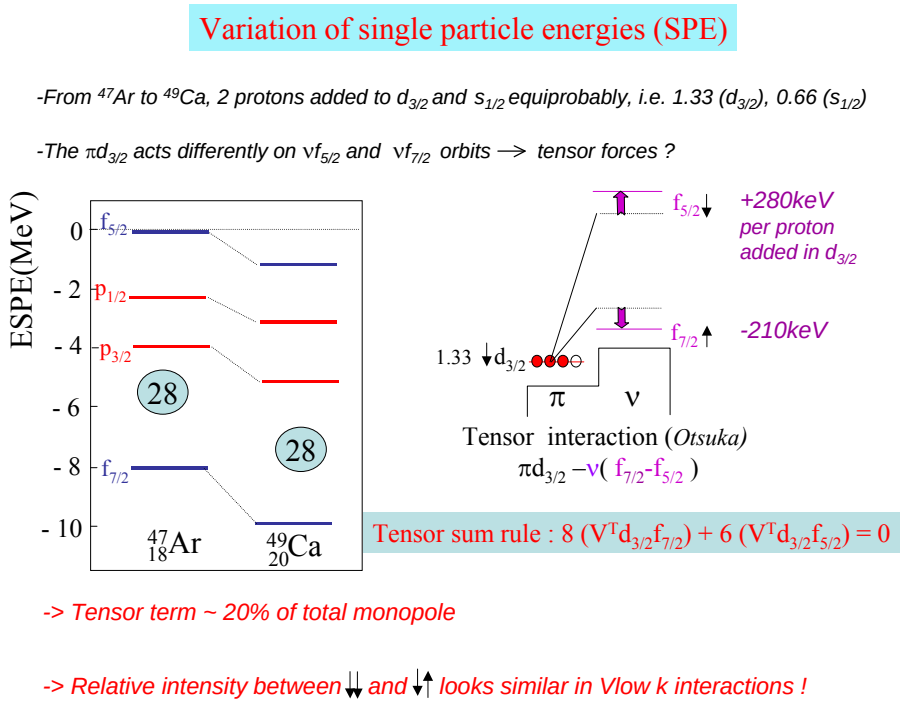

*Figure 2: **Left**: Neutron Effective Single Particle (ESPE) variation between ^{49}Ca and ^{47}Ar derived from the experiment. It is seen in particular that adding two protons to ^{47}Ar gives larger binding energies of the high j components, e.g. $f_{7/2}$. This feature agrees with the property of tensor forces which add an attractive (repulsive) component to the $f_{7/2}$ ($f_{5/2}$) orbit to the spin-independent part of the interaction (see [Otsu01]). **Right**: The effect of the tensor component of the monopole interaction is schematically shown. It leads to a global increase of the spin orbit splitting between ^{47}Ar and ^{49}Ca.*

Therefore to deduce the ESPE of these states, it is necessary to unfold from the correlation effects which are present in most of the nuclei. In practice the shell model monopoles can be adjusted in order to reproduce the energy of the states where the major part of the strength is found. It is then controlled

[9] The coupling of a $p_{3/2}$ neutron with the 2^+ excitation of the core gives rise to several states with J values between $1/2^-$ and $7/2^-$, with which the single particle states $1/2^-$, $3/2^-$, $5/2^-$ and $7/2^-$ can interact, modifying their intrinsic composition.

that the effect of correlations is able to reproduce the remaining fractions of the single particle strengths. In the present case, a remarkable agreement was found between experiment and shell model calculation leading to the neutron ESPE evolutions given in the left hand side of Figure 25.
One sees that the addition of 2 protons between these 2 nuclei leads to a different displacement of the neutron $f_{7/2}$ and $f_{5/2}$ orbits, the $f_{7/2}$ becoming much more bound relatively to the $f_{5/2}$ one. This indicates the existence of a spin-dependent proton-neutron interaction, which binds more the $f_{7/2}$ and slightly repulses the $f_{5/2}$ neutron orbits as compared to a global spin independent interaction. This can be partly accounted for by tensor forces. By adding $d_{3/2}$ protons, the $d_{3/2}f_{7/2}$ proton-neutron tensor interaction V^T has an attractive component quantified here to -210 keV, whereas the $d_{3/2}f_{5/2}$ has a repulsive one, quantified to about +280 keV [Gaud06]. These values correspond to about 20% of the total proton-neutron interaction (monopole) which is globally attractive. These intensities of V^T should fulfil the tensor sum rule [Otsu01]:

$$8(V^T d_{3/2}f_{7/2}) + 6\,(V^T d_{3/2}f_{5/2}) = 0.$$

This rule means that for spin-saturated shells (in which the upper and lower j components are filled completely), the net effect of the spin-dependent tensor interaction should be zero as the two components compensate. Spin-dependent forces lead to a reduction of the N=28 gap by about 330 keV and of the $p_{1/2}$-$p_{3/2}$ neutron SO spacing by about 200 KeV[10] from ^{49}Ca to ^{47}Ar.
To summarize, reduction of SO and of the N=28 gap are found from ^{49}Ca to ^{47}Ar by removing 2 protons from the sd shells. When going from ^{47}Ar to ^{43}Si, 4 protons are expected to be removed from the degenerate $d_{3/2}$ and $s_{1/2}$ protons shells. Assuming that nuclear interactions do not change as a function of the binding energy of the shells, modifications already started between ^{49}Ca to ^{47}Ar will be pursued further down [Sorl10]. A global compression of the ESPE follows, with a weaker N=28 gap as shown in Figure 26.

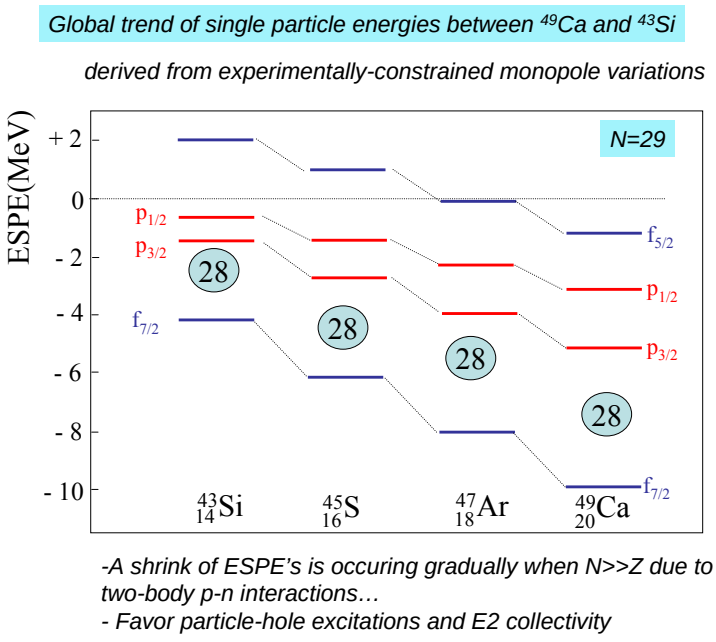

Figure 26: Evolution of ESPE extrapolated from the experimental trend derived from ^{49}Ca to ^{47}Ar. A global squeezing of the orbits is seen, encouraging particle hole excitations across the N=28 gap.

[10] The reduction of the $p_{1/2}$-$p_{3/2}$ neutron SO splitting does not originate from the tensor force, as the proton $s_{1/2}$ orbit has no preferred orientation. Rather it comes from the two body spin orbit interaction due to the removal of a fraction of $s_{1/2}$ protons. As the s orbit is the only one occupying the centre of the nucleus (as encountering no centrifugal barrier), this neutron SO reduction is ascribed to a central depletion of the nuclear density. If confirmed, this effect would corroborate the early definition of the spin-orbit interaction as the derivative of the nuclear density.

This compression of levels will further encourage cross-shell excitations, already visible in ^{46}Ar at the 1p1h level, to develop. As mentioned earlier, correlations of quadrupole nature will develop, making potentially the ^{43}Si nucleus a very deformed nucleus. The ^{44}S nucleus, which sits in between, would have an intermediate configuration combining spherical and deformed shapes. Searches for (i) a shape transition or coexistence in ^{43,44}S as well as (ii) a strong deformation of ^{42}Si have been carried out at GANIL. The low-lying isomers observed in ^{43}S [Gaud09] and ^{44}S [Forc09] were interpreted as witnesses of shape coexistence.

The search for the first 2^+ state in ^{42}Si was carried out at GANIL using the double step in-beam fragmentation technique [Bast07]. A high intensity primary beam of ^{48}Ca was used to produce a cocktail of nuclei among which ^{44}S was used to induce a secondary reaction to produce ^{42}Si by the knock-out of 2 protons. The large efficiency gamma array château de crystal consisting of 70BaF_2 detectors (about 50% at 1MeV) was placed around the secondary target to collect gamma-rays emitted in flight and produced during the prompt de-excitation of the ^{42}Si fragments. The single peak observed at about 770 keV is ascribed to the de-excitation of the first 2^+ state, as shown in Figure 27. When placed in the systematics of 2^+ energies in the Ca and S chains, it is seen in the right part of Figure 27 that the ^{42}Si nucleus is the most collective, having the smallest 2^+_1 energy value in this mass region. The underlying mechanism for the appearance of deformation is likely to be due to tensor forces. Their net effect on the neutron $f_{7/2}$ orbit is zero in ^{48}Ca as far as the two protons SO partners $d_{3/2}$ and $d_{5/2}$ are filled, as given by the tensor sum rule mentioned above. The removal of $d_{3/2}$ protons (from ^{48}Ca to ^{42}Si) therefore provokes a spin asymmetry leading to dramatic changes in the neutron single particle energy values. The decomposition into central, spin-orbit and tensor interaction of the monopoles involved in the sdpf valence space can be found in Ref. [Smir10] and in the lecture of N. Smirnova to the present Ecole Joliot Curie school. The effect of the tensor interaction to modify the N=28 gap and the SO splittings is shown in the bottom of Figure 27.

The SO magic numbers observed in the valley of stability exists because the systems are spin-saturated. In strongly spin-unsaturated systems the spin-orbit splittings are drastically reduced. Meanwhile the shell gap decreases more moderately, but enough to favour deformed states to appear associated to particle-hole excitations over the spherical configuration. While the gap is reduced, the net energy needed to promote particles in the upper shell is reduced, while the amount of correlations generated when the shell is no longer completely filled increases.

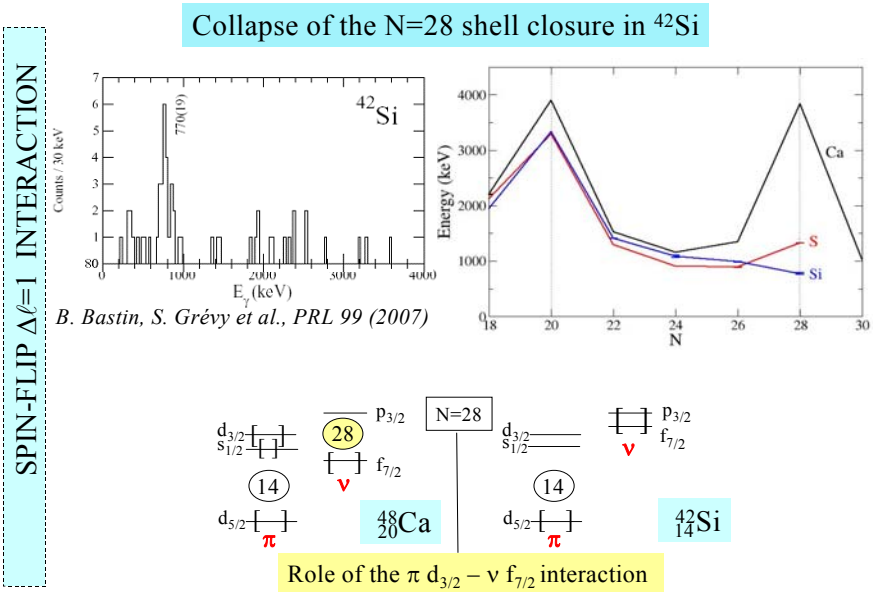

Figure 27: ***Top Left****: Gamma energy spectrum obtained during the -2p knock-out reaction $^{44}S \rightarrow ^{42}Si$. A peak is observed at 770keV, which is ascribed to the $2^+_1 \rightarrow 0^+$ transition in ^{42}Si [Bast07].* ***Top Right****: Evolution of 2^+_1 energies for the Ca, S and Si isotopic chains. If a remarkable 2^+_1 peak is consistently seen at N=20, a decrease of 2^+_1 is seen instead at N=28.* ***Bottom****: Schematic picture showing the role played by the proton-neutron $d_{3/2}$-$f_{7/2}$ interaction in modifying the size of the N=28 gap.*

Evolution of SO-like shell gaps due to proton-neutron $\Delta\ell$=1 interactions

From Figure 19 the disappearance of the Harmonic oscillator shell closures was ascribed to the effect of nuclear forces between spin-flip proton-neutron orbits having the same angular momenta, e.g. $d_{3/2}d_{5/2}$. For the spin-orbit category of magic shells, we rather invoked the effect of nuclear forces between spin-flip proton-neutron orbits having angular momenta differing by one unit of angular momentum, e.g. $d_{3/2}f_{7/2}$. Even if the spin-induced effect is weaker in the case of $\Delta\ell$=1 than in $\Delta\ell$=0 due to the fact that the former have weaker spatial overlapping wave functions, one could wonder if this mechanism provoking the erosion of the N=28 shell closure is universal or not[11]. As shown in Figure 28, the SO magic numbers are large when tensor forces are neutralized, i.e. when the two proton orbits with spin up and down are filled. This holds true in particular for ^{22}O, ^{48}Ca, ^{90}Zr, and to a weaker extent in ^{152}Gd. Whether this mechanism is strong enough to destroy the magic shells depends on the size of the shell gap and the strengths of the nuclear interactions involved to reduce it. We saw that the spherical shell gap is reduced at N=28, and the same observation was derived at N=14 through the observation of the very small 2^+_1 energy in ^{20}C [Stan09]. For higher ℓ orbits , the spin-orbit force is larger and the size of the N=50 and 82 shell gaps are of the same order of magnitude as the N=14 and N=28 ones. However the strength of the monopole terms is reduced as the nucleus grows in size, making them less vulnerable to erosion. In particular experimental data are in favour of a large N=82 gap in ^{132}Sn. The ^{78}Ni case is intermediate between N=28 and N=82, therefore it is hard to predict if ^{78}Ni will be a truly spherical rigid nucleus, exhibit shape coexistence or be deformed.

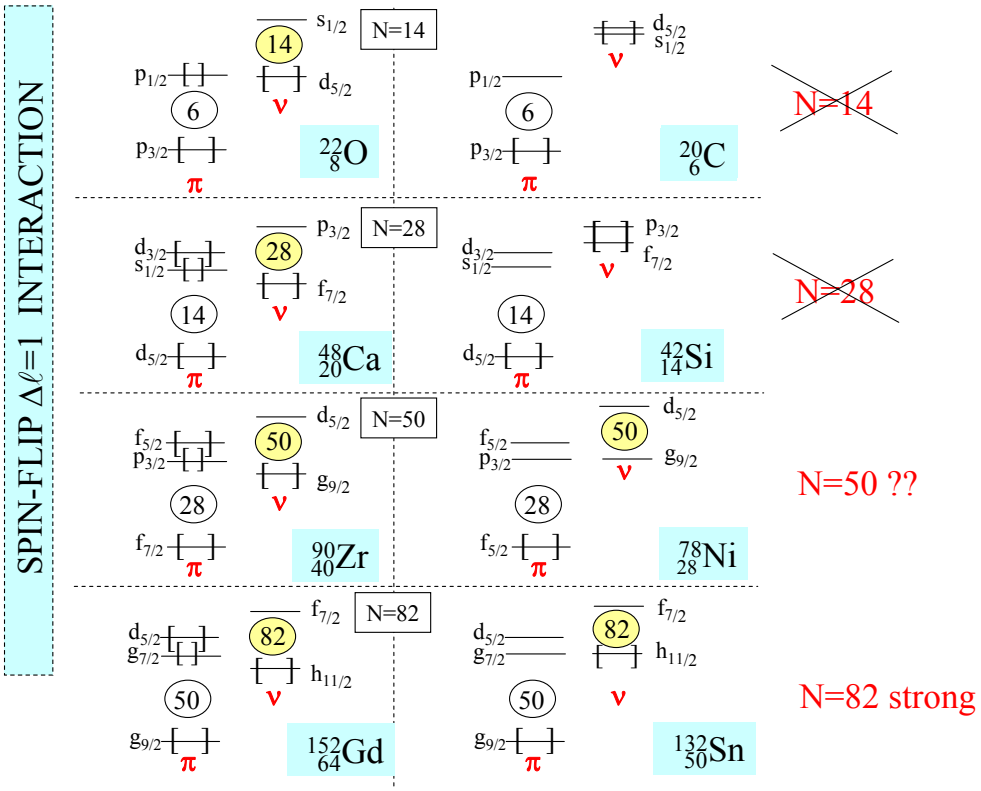

Figure 28: Schematic view of the proton-neutron interactions between orbits separated by one unit of angular momentum. It is seen in particular that for the proton spin-saturated cases (on the left hand side) the N=14, 28, 50 and 82 shell gaps exist (from the top to the bottom part of the Figure). By making the system spin-unsaturated (right hand side) the N=14 and N=28 shell gaps vanish. On the other hand the N=82 is preserved. The behaviour at N=50 (for ^{78}Ni) is expected to be intermediate between N=28 and N=82.

[11] Note that the intensity of the tensor interaction and its ability to modify shell gaps is already found in the bare interactions [Otsu10]. This remark does not hold for the central part of the nuclear interaction.

Take away message – Part III and IV

Key information derived from the evolution of the N=20 and N=28 shell gaps

- The neutron-neutron (T=1) monopole matrix elements are usually repulsive, with the exception of the ones involving pairing interaction, i.e. $Vd_{5/2}d_{5/2}$, $Vf_{7/2}f_{7/2}$

- These peculiar two-body matrix elements are responsible for the creation of the major SO-like shell gaps ($Vd_{5/2}d_{5/2}$ for N=14, $Vf_{7/2}f_{7/2}$ for N=28, $Vg_{9/2}g_{9/2}$ for N=50…[Sorl08]) which are neither reproduced by mean field calculations nor by the two-body interactions derived from bare NN interactions (see Figure 22). This latter feature calls for a better understanding of the pairing interaction [Hebe09], or/and for the use of three-body forces to model the properties of T=1 interactions [Otsu10b,Schw10]

- Proton-neutron interactions between spin-flip partners (nucleons having opposite spin-direction) with angular momenta $\ell_\pi = \ell_\nu$ or $\ell_\pi = \ell_\nu \pm 1$ and the same number of nodes n_π=n_ν are more attractive than others. Consequently these interactions play an essential role to modify the HO and SO-like magic numbers, respectively, throughout the chart of nuclides. It has in particular been identified that the proton-neutron interaction $Vd_{5/2}d_{3/2}$ is important to change the N=20 shell gap, leading to the deformation of ^{32}Mg. On the other hand the $Vd_{3/2}f_{7/2}$ modifies the N=28 shell gap to induce deformation in the ^{42}Si nucleus. While all HO-like shell gaps 8, 20, 40 are modified in the same manner by the $\ell_\pi = \ell_\nu$ interaction (see Figs.19, 20), the modification for the SO-like magic numbers is no longer decisive at N=82 (see Fig. 28)

- Modifications of the NN interactions are also expected by the proximity of continuum states. In particular, the interaction between a well bound proton and a weakly bound or unbound neutron should be reduced as compared to the one between two well bound nucleons. In a first order, this arises from the fact that the radial wave function of the neutron (which is not sensitive to the Coulomb barrier) can extend further out of the nuclear potential well of the nucleus, hereby having a smaller overlap with the wave function of a well bound proton located in the interior of the nucleus. This effect is not yet systematically taken into account nowadays, but experimental data are searched for to compare to theories under development, such as the ones based on the continuum shell model approach for light systems [Doba07]

PART V: INTERPLAY BETWEEN THE ASTROPHYSICAL R-PROCESS AND NUCLEAR STRUCTURE

As mentioned along the previous chapters the properties of NN interactions, such as those of the tensor forces, can significantly alter or reinforce the strength of a shell closure. In addition, the change of the mean field potential of the nucleus, in particular the increased surface diffuseness for weakly bound systems having large N/Z ratios [Doba94], also modifies the energy of the orbits. Taken together with a profound change of the spacing and ordering of levels may occur when moving from stability to the drip line, following for instance a given isotonic chain. The present section shows how these structural changes impact the development of the rapid-neutron capture nucleosynthesis (r-process). For further details we refer the reader for instance to Refs. [Pfei01,Krat07,Graw07] for review papers.
After a brief introduction on the role of this process and the possible astrophysical sites where it may occur, the key nuclear structure parameters (binding energy, beta-decay lifetime and neutron capture cross section) to its development will be discussed. Nuclear structure evolution can modify these parameters significantly, changing in turn the location and duration of the r process. Enlighten by the previous chapters on the evolution of shell closures, expected modifications of the N=82 gap will be commented and put in an astrophysical perspective.

Introduction to elemental abundances

The quest for the origin of the chemical elements has been a fascinating subject of philosophical, theological and scientific debates for centuries. The first decisive attempt to interpret the observed elemental composition from nuclear physics concepts was made by the fundamental paper of Burbidge, Burbidge, Fowler and Hoyle [B2FH]. This work sets the starting of Nuclear Astrophysics, an interdisciplinary field which merges astronomical observations, astrophysical modelling, meteoritic research, and nuclear physics.
The credibility of any nucleosynthesis model must be checked against observations. The sun was considered for a long time as a suited choice for determining the abundance of the elements, being the only sample for which we can determine a well defined isotopic composition throughout the periodic table of the elements. This point is crucial since the final isotopic abundances reflect the nuclear reactions they were formed in. However, several stellar processes mixed during the formation of the proto-solar nebula and built up the solar elemental abundance. It is, therefore, almost impossible to disentangle the various nucleosynthesis events which occurred in the solar system prior to its formation.

There is an active search for weakly mixed abundances which contain contributions from few sites only. One possibility is to observe stars formed at the beginning of the galactic evolution, when very little nucleosynthetic processes had yet occurred. During galactic chemical evolution, the content of elements heavier than H and He in the interstellar medium is increased by stellar hydrostatic and explosive burning processes. Thus, abundance ratio such as Fe/H can be used as an indicator to probe the amount of nucleosynthetic processing that occurred for the elements found in a given star.
The discovery of ultra metal-poor (UMP) stars in the galactic halo (Fe/H < 1/1000 of the Sun) has been a major breakthrough in astronomy, revealing the galactic composition at an early age [Sne98,Tru01,Cow02].

Another possibility is brought by the abundance patterns of certain refractory inclusions of meteorites or presolar grains which exhibit large isotopic anomalies with respect to solar [Clay,Besm03,Ama03]. These observations indicate that their abundances have not been completely dissolved when incorporated to the solar nebula. They still carry fingerprints of the precursor exploding star from which pieces of matter have been ejected. They subsequently cooled and condensed into microscopic grains travelling through the interstellar medium, being eventually enclosed in other material, forming solid rocks and collected on Earth in the form of meteorites.

Introduction to the r process nucleosynthesis

The relative abundances of nuclides observed in the solar system (shown in the left part of Figure 29) displays distinct patterns carrying imprints of the processes involved to create these elements. A steep decrease in abundance is seen below Fe. This rapid fall-off witnesses the fact that these elements are mainly produced by fusion reactions, which require the tunnelling through an increasing Coulomb barrier as Z increases. The Fe peak is created at the end of an equilibrium process between charged particles and photodisintegrations reactions which favour the productions of the most bound elements in nature, i.e. around Fe. Above Fe a smooth fall-off in abundance is found, indicating that charged particles are no longer involved there but neutron captures, which are not sensitive to the Coulomb barrier, take over. Therefore the abundance curve stays almost constant as a function of Z or A, except when shell closures are present. There, the neutron-capture cross section decreases by several orders of magnitude immediately after having passed the shell gap. It follows that nuclei at closed shells have a much larger abundances than their neighbours, leading to the presence of three distinct twin peaks superimposed on the smooth abundance curve. Each peak has a narrow width at stable nuclides with magic neutron numbers N=50, 82, and 126, and a broader peak shifted to slightly lower mass numbers as shown in the left part of Figure 29. This indicates the existence of (at least) two components, attributed to slow (s) and rapid (r) neutron-capture nucleosynthesis.

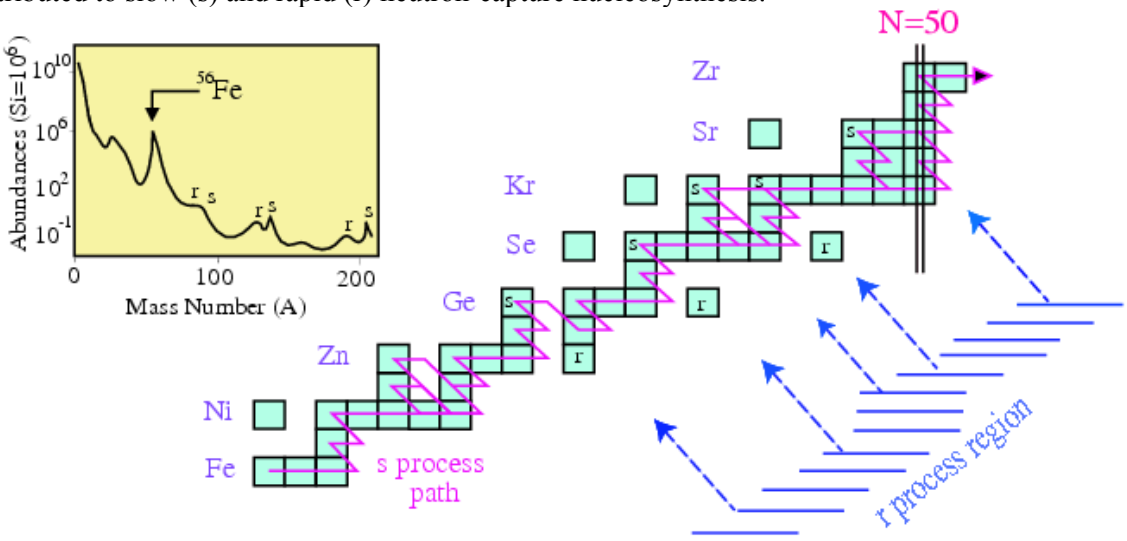

Figure 29: ***Top Left****: Solar abundance curve of the elements, normalized to Si.* ***Center****: The s process path, corresponding to given density and temperature, is shown in pink. It develops in the valley of stability. Therefore the most neutron-rich nuclei such as ^{70}Zn, ^{76}Ge and ^{82}Se cannot be reached by this process. Rather the r process, which is driven further from the valley of stability is producing these pure r isotopes.*

A typically expected s process path is shown in Figure 29. It operates in red giant stars at relatively low neutron density of about $10^8 cm^{-3}$, with neutron captures lifetimes on seed nuclei typically longer than their β-decay lifetimes $T_{1/2}$. As a consequence, the s-process path follows the valley of stability and isotopes with small neutron-capture (n,γ) cross section σ_n are greatly enhanced [Kapp99]. Along the s process path, we find approximately that the product of the cross section and abundance $\sigma_n N_s$ is constant. Small (n,γ) cross sections are encountered for closed shell nuclei, leading to the building of s-process peaks (right part of the twin peaks displayed in Fig. 29) at atomic masses A=88, 140, and 208. Most of the cross sections of the stable nuclei involved in the s process have been measured with an accuracy of about 10%, with some exceptions. Using these cross sections, the fraction of s elements in the total abundance curve can be derived. The remaining part of the observed elements above Fe is ascribed to the r process.

The other half of the elements beyond Fe (as in particular the most neutron-rich) is supposed to be produced via neutron captures on very short time scales in neutron-rich environments. In very hot and neutron-dense environments, the r-process proceeds very far off stability. The r-progenitors subsequently β-decay to enrich the stable elements in the valley of stability. As shown in Figure 29, some neutron-rich stable isotopes (^{70}Zn, ^{76}Ge and ^{82}Se) have purely r component as the s process cannot reach them. These stable isotopes are shielding the corresponding isobars from being produced by the r process as well. Therefore ^{70}Ge, ^{76}Se and ^{82}Kr have a pure s process origin.

Despite its importance, the exact site(s) where the r-process(es) occurs still remain one of the greatest mystery in science. The most frequently suggested astrophysical environments are high-entropy ejecta from type II supernovae (SN) [Woos94] and neutron-star mergers [Frei99]. The shock-heated He or C outer layer of type II SN could provide a moderate neutron flux (a weak r-process) through ^{13}C(α,n) reactions which could account for several isotopic anomalies found in pre-solar grains. The key for understanding the r-process(es) resides in a close interaction between astronomy, cosmochemistry, astrophysical modelling of explosive scenarios and nuclear physics. Only the nuclear structure aspects will be discussed here.

To account for the production of r-peaks, shifted to lower atomic masses as compared to the s process, neutron-rich nuclei should be produced. In a very hot and neutron-rich environment, the rate of captures is balanced by that of photodisintegrations induced by the ambient photon bath of the exploding star. The corresponding ratio of nuclei N(A+1)/N(A) depends on the neutron density d_n, the temperature and the neutron separation energies S_n(A+1). Its is given by the so-called Saha equation, which is deduced from the Boltzmann population rule :

$$\frac{N(A+1)}{N(A)} \propto d_n \exp(-S_n(A+1)/kT)$$

This equation means that, for a fixed temperature and neutron density, the abundance in a given isotopic chain is determined by the S_n values. For $d_n \sim 10^{24}$ cm^{-3} and T~10^9K, it is found that the r process is reaching nuclei with small binding energy (S_n ~ 2-3MeV). As a sharp drop of S_n(A+1) occurs after a major closed shell, an accumulation of nuclei is found there. The process is then stalled at these so-called waiting-point nuclei until beta decays occur, depleting the nucleosynthesis to the upper Z isotopic chain where a subsequent neutron-capture could immediately occur. After successive beta decays and neutron captures at the N=82 closed shell, the process is progressively driven closer to stability at higher Z where β-decay lifetimes $T_{1/2}$ become longer (see the red zig-zag line along the N=82 shell in Figure 30). There, around the Sn isotopic chain, neutron captures are expected to proceed faster than photodisintegration and beta-decay rates, possibly driving the r-process nucleosynthesis towards the next shell closure.

At the end of the r-process, radioactive progenitors decay back to stability via beta or beta-delayed neutron emission. The accumulation of r-elements which form the r-peaks at masses A~ 80, ~130 and ~ 195 on the abundance curve of the elements is a direct imprint of the existence of waiting point progenitors far from stability. The location, height and shape of the A=130 peak could be traced back from the neutron separation energies (S_n), the half-lives ($T_{1/2}$), the neutron delayed emission probability (P_n), and the neutron-capture cross section (σ_n) of the nuclei located at the N=82 shell closure. These parameters are imbricated in the structural evolution of the nuclei as depicted in the following paragraph.

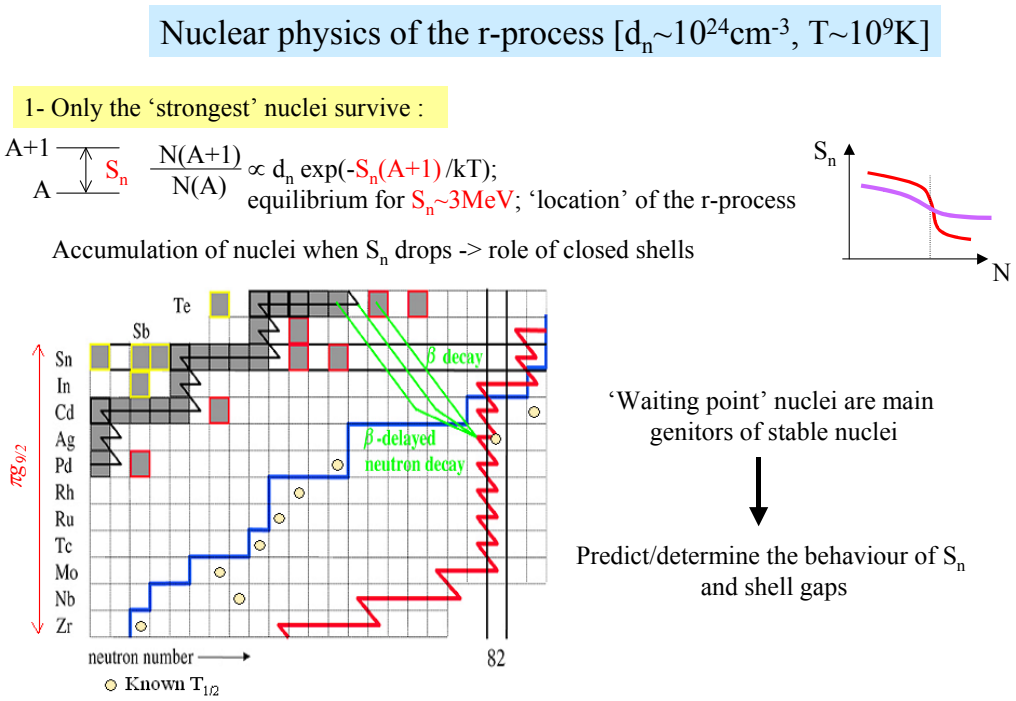

Figure 30: ***Top Left****: Relationship expressing the Boltzmann population of two states (here the abundance of A+1 and A nuclei) separated by an energy $S_n(A+1)$ as a function of neutron density d_n and temperature T.* ***Top Right****: Schematic variation of S_n for a strong shell closure (in red) or for a quenched shell closure (in purple). For the first case, the r progenitors are well located at the shell closure, while for the second the r progenitors are more spread along the isotopic chain.* ***Bottom Left****: Schematic representation of the location of the r-process path (in red) at the N=82 shell closure for a given neutron density value and assuming a strong shell closure. The present experimental knowledge on the atomic masses is indicated by a thick blue line. As far as β-decay lifetimes are concerned, measurements (shown with yellow circles) extend further from stability, reaching in particular the ^{130}Cd [Dill03] and ^{129}Ag waiting-point nuclei [Dill03,Pfei01,Kra05].*

Influence of nuclear structure on the r-process nucleosynthesis

The evolution of the N=82 shell gap south to the doubly magic nucleus $^{132}Sn_{82}$ is ruled by the combined effects of the proton-neutron interactions and by the progressive proximity of the continuum states. From Z=50 to Z=40 only the proton orbit $g_{9/2}$ orbital is progressively emptied (see the right part of Figure 32), therefore all the proton-neutron monopole interactions which intervene in the evolution of nuclear structure between $^{132}Sn_{82}$ and the close-to-drip-line nucleus $^{122}Zr_{82}$, involve the same proton orbit. As shown schematically in the right part of Figure 32 some monopole interactions can play an important role to modify the ordering of the neutron orbits, hereby possibly reducing the size of the N=82 shell gap as protons are removed from Z=50 to Z=40. Related to this reduction, the tensor interactions (through the $\pi g_{9/2}$-$\nu h_{11/2}$ or $\pi g_{9/2}$-$\nu f_{7/2}$ monopoles) are likely to play the most important roles.

The role of atomic masses

The influence of the S_n values on the r-abundance peaks at the N=82 shell closure has been emphasized in Refs. [Chen95,Pfei01]. Using mass models which give rise to strong shell closures (as FRDM or ETFSI-1), one obtains a local increase of the S_n values around N=70 and a very abrupt drop immediately after N=82. They originate from a predicted strong quadrupole deformation around ^{110}Zr and a strong shell closure at N=82, respectively. As a result, neutron captures are stalled for a while around A=110, N=70 and are subsequently directly driven to the closed shell N=82. This leaves few r-

progenitors in between these two regions, leading to a significant trough in the fit of the abundance curve of the elements at A~120 in Fig. 31[12]. On the other hand, models exhibiting less strong shell closures (called "quenched" mass models as ETFSI-Q or HFB/SkP) lead to a smoothened variation of S_n values, bringing back r-progenitors before reaching the N=82 shell closure[13]. Thus the trough at A~120 is filled in closer agreement with the solar r-abundance curve[14]. The recent determination of the Q_β-value in the β-decay of the ^{130}Cd [Dill03] waiting-point nucleus as well as the study of the ^{131}In isomer [Gors09] accredit this weakening which should however be confirmed by further investigations. From these arguments, it follows that the determination of the S_n values at the N=82 shell closure is essential. So far theoretical models diverge soon after departing from the last measured nucleus, as discussed for instance in Ref. [Lunn03], meaning that the underlying physics which could modify the binding energies of the orbits is poorly known and far from being consensual.

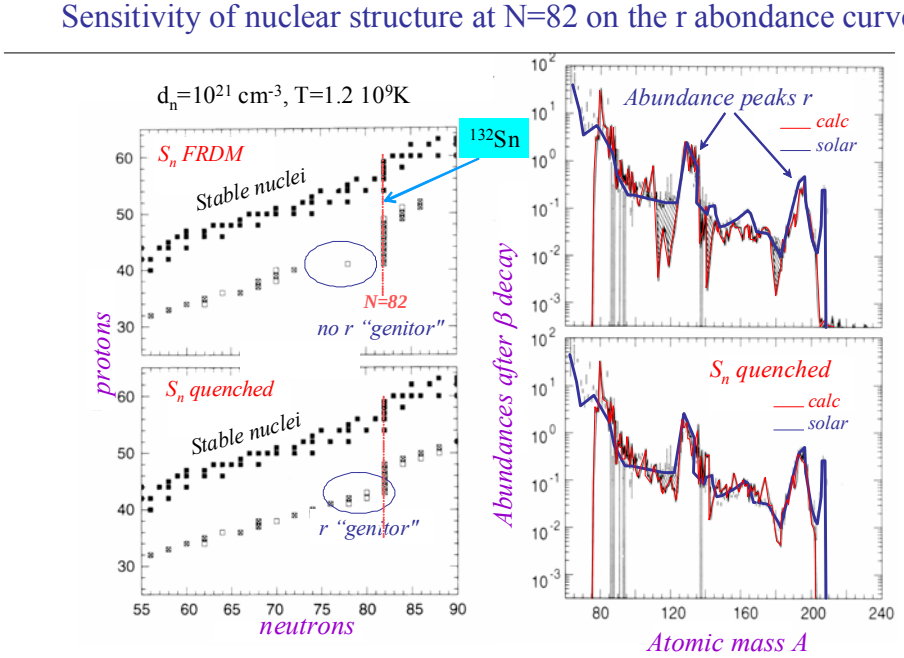

Figure 31: ***Left*** *Major r process progenitors are indicated with open squares (with a cross 90%, without 10% of total abundance) for given neutron-density and temperature conditions, assuming a strong N=82 shell closure, as found by the Finite Range Droplet Model [Moll85], or by the HFB/SkP [Doba96] model which gives quenched shell gaps.*
Right*: The corresponding calculated abundances of the elements using the Saha equation (compared to solar abundances). For the strong shell closure hypothesis (upper part), the neutron capture flow is immediately driven to the N=82 shell, leaving few progenitors before. This produces a hole in abundance before the major r peaks. Rather the quenched mass formula (lower part) is filling these holes (adapted from Ref. [Pfei01]).*

The role of β-decay lifetimes

Likewise, the strength of the tensor interaction influences strongly the β-decay lifetimes of the N=82 nuclei through the $\pi g_{9/2}$-$\nu g_{7/2}$ monopole, as depicted in Figure 32. Indeed the β decay of N~82 nuclei south to Z=50 proceeds mainly through the Gamow-Teller (GT) transition $\nu g_{7/2} \rightarrow \pi g_{9/2}$ transition, as

[12] Noteworthy is the fact that if ^{110}Zr were a doubly magic nucleus, a sudden drop of S_n value at N=70 would be found, leading to the build up of r-process elements at A~110.
[13] The reduction of the shell gap can occur from the action of proton-neutron two-body forces, combined with the change of single particle energies induced by the increased diffuseness of the nuclear potential well for the neutrons. Here the term "quench" includes both effects, which still have to be proven experimentally.
[14] Note that this better agreement does not necessarily documents for quenched shell closures, as a specific stellar origin could account for the filling of these mass regions as well.

described in Refs. [Dill03,Cuen07]. The $\nu h_{11/2} \rightarrow \pi g_{9/2}$ first forbidden decay transition is expected to contribute to less than 10% of the beta-decay lifetime [Cuen10]. As protons are progressively removed from the $g_{9/2}$ orbit, the neutron $g_{7/2}$ orbit becomes gradually less deeply bound due to the missing proton-neutron interactions $\pi g_{9/2}$-$\nu g_{7/2}$. Consequently, the aforementioned GT transition will occur at gradually smaller excitation energy E^* in the daughter nuclei, leading to a drastic shortening of β-decay lifetimes $T_{1/2}$, which scales with $1/(Q_\beta - E^*)^5$.

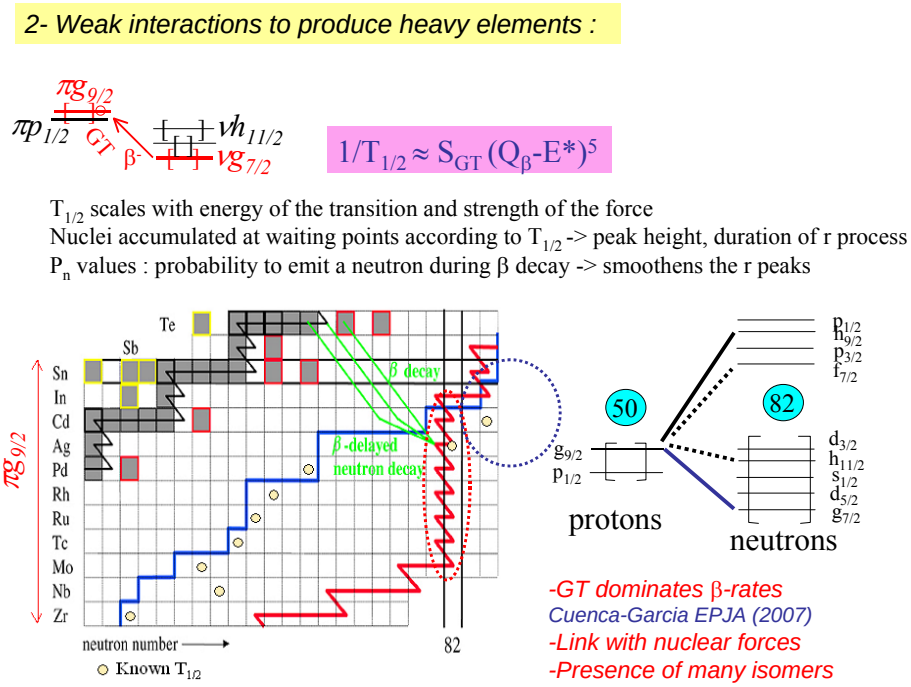

Figure 32: Schematic view of the proton-neutron interactions which play a role for the evolution of the β decay lifetime $T_{1/2}$. ***Bottom right****: The interaction between the π $g_{9/2}$ and ν $g_{7/2}$ orbits, indicated by a full line, is expected to be the largest among all other interactions involved, see text for explanation and consequences. The dashed (full) lines indicate proton-neutron interaction containing a repulsive (attractive) tensor force. This tensor part will influence the absolute value of the nuclear interaction. The loci indicated in red and blue on the chart of nuclides correspond to the approximate locations where lifetimes play the most important role.*

When short-lived nuclei are paving the r-process path, the abundance peaks of the r-elements are barely formed and a total duration of the explosive process of few milliseconds could be long enough to reach the heaviest elements of the chart of nuclides. At the opposite, long-lived nuclei located in the r-process path are the major genitors of stable r-nuclei in the universe, after series of β or β-neutron decays to stability, and are responsible for the existence of significant peaks in the abundance curve of the elements. Therefore accurate half-life predictions or measurements are required along the r-process both to explain the shape of observed peaks but also to constrain the duration of the r-process.
When the β-decay partly proceeds above the neutron emission threshold of the daughter nucleus with a probability P_n, a neutron is emitted after the conversion of a neutron into a proton by the β^- decay process. In such a process a nucleus (A,Z) is therefore converted to (A-1,Z+1) with the fraction P_n, and to (A,Z+1) with the probability $1-P_n$. This delayed neutron emission probability smoothens the abundance curve of the elements as the decay can proceed to masses A and A-1. It follows that the abundance curve of the elements no longer exhibits an odd-even effect abundance pattern as for the s peak. A review of the measured lifetimes relevant for the r process, as well as the role of isomers which can be thermally populated in exploding stars, can be found in Ref. [Kra05]. So far, most of the lifetime measurements relevant for the r process have been achieved at the ISOLDE/CERN facility.

The role of continuum

Added to the properties of the NN interactions which are assumed for the moment to be unchanged whatever the respective binding energies of protons and neutrons are, self-consistent mean-field

calculations which encompass the treatment of continuum states show a quenching of the N=82 shell gap when approaching the neutron drip-line [Doba94]. This is primarily caused by the lowering of the low *j* orbits relative to high-*j* ones. The low-*j* neutron orbits, such as the $\nu p_{1/2}$ and $\nu p_{3/2}$ ones, may progressively become the valence states immediately above the N=82 gap. Such effects were ascribed to the fact that, close to the drip-line, the low-*j* neutron orbits of the continuum interact strongly with bound states, whereas the interaction with the high-*j* ones is much less effective. Qualitatively, the nuclear mean field close to the drip-line could be mimicked by a Nilsson potential without the ℓ^2 term [Doba94]. At exploding star temperatures of typically 10^9K (or neutron energies of about 100keV) neutrons can hardly overcome large centrifugal barriers created by high ℓ orbits. Therefore, the presence of low-*j* or low-ℓ neutron valence orbits at low excitation energy would enhance the neutron capture cross-sections σ_n by several orders of magnitudes, shortening the neutron capture time at the waiting-point nuclei accordingly.

The role of neutron capture cross sections

Neutron capture cross-sections are often calculated in the framework of the statistical Hauser-Feshbach model [Haus52,Cow91,Raus97], which assumes the presence of a high density of states above the neutron separation energy with various spin and parity values (see Figure 33). However the use of this statistical approach is no longer appropriate to calculate neutron capture cross sections for neutron-rich nuclei at closed shell, since the neutron-separation energy is small and the level density is low. In such cases, the main contribution is obtained from direct captures on few bound states of low ℓ values, mainly through *s* or *p* waves, or/and by resonant captures slightly above the neutron-energy threshold (see Figure 33).

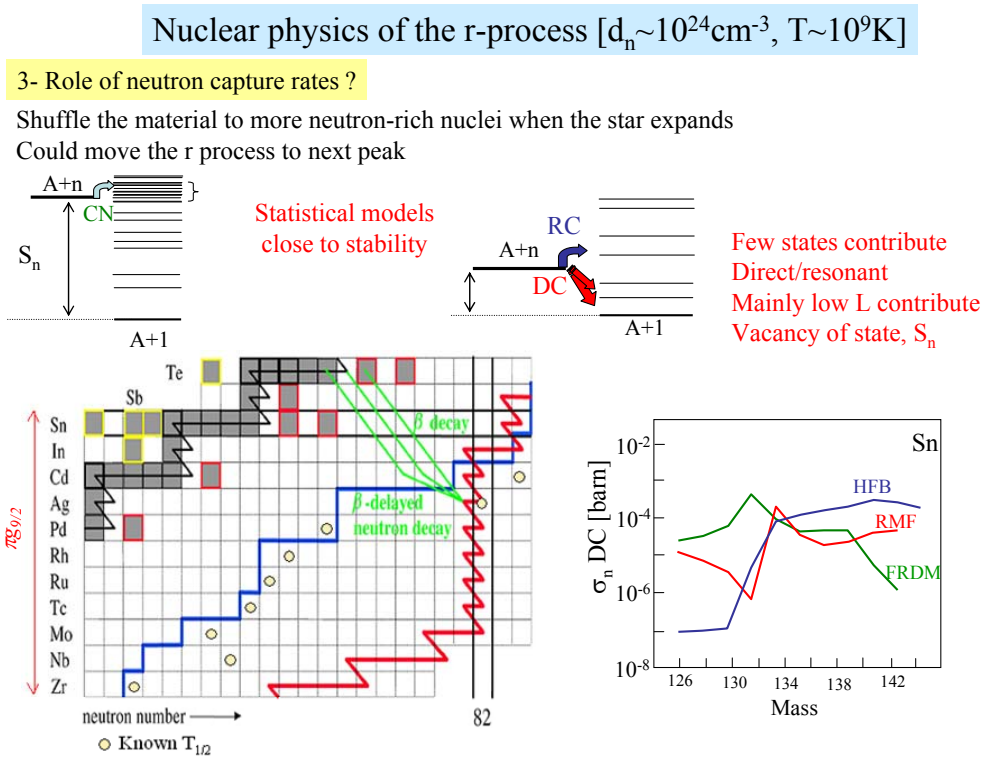

Figure 33: ***Top****: Schematic views of the processes through which neutron captures can occur are shown. On the* ***left****, the formation of a compound nucleus is favoured, leading to a treatment of the neutron capture by the Hauser-Feshbach statistical model. On the* ***right****, the resonant and the direct capture processes dominate for neutron-rich nuclei at closed shells. Capture to low ℓ states gives larger cross sections, as the centrifugal barrier is low.* ***Bottom right****: Neutron capture predictions using various mean field models show discrepancies of up to two orders of magnitude, emphasizing the importance of having reliable nuclear physics values of the energy of the states, spectroscopic factors and atomic masses [Raus98].*

The fact that the neutron *p* orbits become the few first valence states is therefore extremely important. This feature is discussed in Ref. [Raus98] for the ^{133}Sn nucleus above N=82. In Figure 33, it is shown that predictions on direct neutron-capture rates can differ by up to two orders of magnitude in this mass region.
As the direct capture cross section proceeds mainly through the same $\nu p_{3/2}$ and $\nu p_{1/2}$ states from Z=50 down to Z=40, the evolution of their energy and spectroscopic factors determines how neutron-capture cross sections will change along the N=82 shell closure. It indicates to which extent the r-process will be blocked at this shell closure when the temperature of the exploding system decreases and photodisintegration become negligible. Since the direct determination of neutron-capture cross sections on very unstable nuclei 'A' is technically not feasible, their determination should be provided by models, constrained by spectroscopic information (such as energy, spin, spectroscopic factors of the bound and unbound levels in the 'A+1' nucleus) obtained by (d,p) transfer reactions. Such pioneering studies have been undertaken for the N=28 shell closure in the neutron-rich ^{48}Ca and ^{46}Ar nuclei where similar *p* states come into play in the neutron-capture cross sections [ngdp]. These neutron-capture studies at the N=82 shell closure are expected to be achieved at the SPIRAL2 facility thanks to the high production rate of N=82 nuclei around Sn and Cd and the suitable energy for transfer reactions.

To summarize this astrophysical part, experimental and theoretical achievements aiming at a comprehensive understanding of the evolution of the N=82 shell closure will provide significant insight to the understanding of the r-process nucleosynthesis, as these topics are intimately entwined.

CONCLUSIONS

The present lecture, given at the Ecole Joliot Curie 2009, intended to present a qualitative view of the effects of nuclear forces on the evolution of shell closures and magic numbers. The presentation of important ingredients, concepts, experimental techniques and examples related to nuclear spectroscopy aimed at encouraging some readers to delve more into this fascinating topic.

As was discussed in the manuscript, the atomic nucleus has very peculiar facets which make it remarkable in the world of quantum physics. To name a few, we remind that:

- (i) the nucleus is composed of two fluids (neutrons and protons), which brings a wealth of nuclear interactions (T=0, T=1, pairing, Wigner effect) and structural effects in various regions of the chart of nuclides
- (ii) the nucleus is generating his own mean field potential, making it subject to structural modifications as shape transitions, as nucleons are added
- (iii) nuclear spectra exhibit single particle states which often mix with collective ones such as vibrations and rotations, making the nuclear spectra often difficult to interpret without the help of advanced theoretical models
- (iv) the nucleus has to be modelled using various approaches to account for cluster structures, weakly bound systems, different symmetry properties

The mean field potential gives rise to irregular spacing between the orbits, leading to shell gaps and magic numbers. For light nuclei up to A~40, magic numbers keep imprint of the Harmonic Oscillator potential well, leading to magic numbers at N or Z = 8, 20 and 40. The spin-orbit (SO) force introduces other magic numbers at 14, 28, 50, 82, and 126. Experimental work carried out worldwide for about 30 years evidence the disappearance of the magic numbers which were well established in the valley of stability. It was soon realized that these modifications of shell gaps are due to specific nucleon-nucleon interactions, which play a role when certain orbits are filled. In particular the spin-flip neutron-proton interaction, in which neutrons and protons have anti-aligned spin orientations, plays a crucial role to modify the HO and SO-like shell gaps. It is also clearly identified that interactions between protons and neutrons having $\Delta\ell$=0 and $\Delta\ell$=1 units of angular momentum affect the HO and SO magic numbers, respectively. The exploration of exotic nuclei has enabled to probe these forces to progressively understand their effects. Among the most remarkable ones, one can quote the emergence of halo nuclei; the islands of inversion at N=8, 20 and 40 in which nuclei suddenly occupy the valence states across the gaps; the proximity of the drip line in the O isotopic chain, the disappearance of the N=28 shell closure in ^{42}Si. The persistence of magic numbers will be searched for in the future for the 'a priori' doubly magic nuclei ^{100}Sn and ^{78}Ni, which encounter the same spin-flip forces as for ^{42}Si. Fascinating also is to realize how the properties of the nucleon-nucleon forces impact the abundance curve of the heavy elements, through their influence on the shell gaps, the beta-decay lifetimes and neutron-capture cross sections. Therefore a better understanding and predictability of nuclear forces should be achieved for both understanding how and in which stellar site heavy elements are synthesized in the universe. Nuclear forces have also a decisive role for the emergence of an island of super heavy nuclei. So far models differ on its location and existence.

Apart from these rather phenomenological considerations, modern theories try to derive the forces that prevail in the nucleus from bare two body nucleon-nucleon interactions. But surprisingly, this procedure cannot so far account for the existence of major shell gaps arising from the SO interaction, as for instance the 14 and 28. This observation is revolutionizing our vision of magic numbers, questioning about the origin(s) of the SO interaction, the role of three body forces, of pairing and more generally the understanding of all facets of the T=1 interaction. Last but not least, while reaching the drip line, nuclear interactions are involving weakly bound nucleons. The force acting on them is expected to be dramatically influenced by the proximity of continuum, modifying in turn the shell gaps. With the existing and forthcoming radioactive ion beam facilities worldwide, many aspects of nuclear structure are expected to encounter substantial and exciting developments, e.g. the role of nuclear forces to drive shell evolution, the interplay between the structure and reaction mechanism, the quantum physics related to few body or many body systems inside the nucleus or in the continuum, the

role of symmetries in nuclear structure, the connection between nuclear structure and explosive astrophysical processes, the possibility to produce and study super-heavy elements…

Acknowledgments :

I express gratitude to the scientific committee of the Ecole Joliot Curie for trusting me to give this lecture. D. Lacroix and J.C. Thomas (my shadow lecturer) guided me from the beginning to prepare the oral presentation, and constantly encouraged me to write the course. They are also acknowledged for reading and improving the manuscript. The present work is part of a bigger one on the evolution of shell closures due to the influence of nuclear forces performed in collaboration with M.G. Porquet over two years.

References

[Ama03] S. Amari, *Nucl. Phys. A* **718** (2003) 45c-51c
[B2FH] E. Burbidge, G. Burbidge, W. Fowler and F. Hoyle, *Rev. of Mod. Phys.* **29** (1957) 546
[Bank85] S.M. Banks et al., *Nucl. Phys. A* **437** (1985) 381
[Bast07] B. Bastin et al., *Phys. Rev. Lett.* **99** (2007) 022503
[BE2mg32] T. Motobayashi et al., *Phys. Lett. B* **346** (1995) 9,
H. Iwasacki et al., *Phys. Lett. B* **522** (2001) 9,
B. V. Pritychenko et al., *Phys. Rev. C* **63** (2000) 011305(R),
J.A. Church et al., *Phys. Rev. C* **72** (2005) 054320
[Besm03] A. Besmehn and P. Hoppe, *Geochemica and Cosmochemica Acta*, vol **24** (2003) 4693
[Camp75] X. Campi et al., *Nucl. Phys. A* **251** (1975) 193
[Chen95] B. Chen et al., *Phys. Lett. B* **355** (1995) 37
[Clay] D. D. Clayton and L. R. Nittler, Carnegie Observatories Astrophysics eries, vol 4, Origin and Evolution of the Elements, ed., A. Mc William and M. Rausch (Cambridge University Press).
[Cow91] J. J. Cowan, F.-K. Thielemann and J. W. Truran, *Phys. Rep.* **208** (1991) 267
[Cow02] J. Cowan et al., *Ap. J.* **572** (2002) 861
[Cuen07] J. J. Cuenca-Garcia et al., *Eur. Phys. J. A* **34** (2007) 99
[Cuen10] J. J. Cuenca-Garcia et al., GSI scientific report 2008, p168, Nustar-theory-04
[Dill03] I. Dillmann et al., *Phys. Rev. Lett.* **91** (2003) 162503
[Doba94] J. Dobaczewski et al., *Phys. Rev. Lett.* **72** (1994) 981,
[Doba07] J. Dobaczewski et al., *Prog. Part. Nucl. Phys.* **59** (2007) 432
[Doba96] J. Dobaczewski et al., *Phys. Rev. C* **53** (1996) 1647
[Doll76] P. Doll et al., *Nucl. Phys. A* **263** (1976)210
[Detr79] C. Détraz et al., *Phys. Rev. C* **19** (1979) 164
[Elek07] Z. Elekes et al., *Phys. Rev. Lett.* **98** (2007) 102502
[Fran01] S. Franchoo et al., *Phys. Rev. C* **64** (2001) 054308
[Frei99] C. Freiburghaus, S. Rosswog and F.-K. Thielemann, *Ap. J.* **525** (1999) L121
[Gade06] A. Gade et al., *Phys. Rev. C* **74** (2006) 034322
[Gade08] A. Gade and T. Glasmacher, *Prog. Part. Nucl. Phys.* **60** (2008) 161
[GANIL] D. Guillemaud-Mueller et al., *Phys. Rev. C* **41** (1990) 937,
O. Tarasov et al., *Phys. Lett. B* **409** (1987) 64,
S. M. Lukyanov et al., *J. Phys. G* **28** (2002) L41
[Gaud06] L. Gaudefroy et al., *Phys. Rev. Lett.* **97** (2006) 092501
[Gaud07] L. Gaudefroy et al., *Phys. Rev. Lett.* **99** (2007) 099202
[Gors09] M. Gorska et al., *Phys. Lett. B* **672** (2009) 313
[Graw07] H. Gawe, K. Langanke and G. Martinez Pinedo, *Rep. Prog. Phys.* **70** (2007) 1525
[Guil84] D. Guillemaud-Mueller et al., *Nucl. Phys. A* **426** (1984) 37
[GXPF1] Honma et al., *Phys. Rev. C* **69** (2004) 034335
[Haus52] W. Hauser and H. Feshbach, *Phys. Rev.* **87** (1952) 366
[Hebe09] K. Hebeler et al., arxiv : 0904.3152v2 [nucl-th] Oct 28th 2009, see also T. Duguet's lecture.
[Heis69] J. Heisenberg et al., *Phys. Rev. Lett.* **23** (1969) 1402

[Hoff08] C. R. Hoffmann et al., *Phys. Rev. Lett.* **100** (2008) 152502
[Hub78] G. Hubert et al., *Phys. Rev. C* **18** (1978) 2342
[Kapp99] F. Kaeppeler et al., *Prog. Part. Nucl. Phys.* **43** (1999) 419
[KB3G] E. Caurier et al., *Rev. Mod. Phys.* **77** (2005) 427
[Khan85] S. Khan et al., *Phys. Lett. B* **156** (1985) 155
[Kra05] K.-L. Kratz et al., *Eur. Phys. J. A* **25**, s01 (2005) 633 – 638
[Kram01] G.J. Kramer et al., *Nucl. Phys. A* **679** (2001) 267
[Krat07] K. -L. Kratz et al., *Prog. Part. Nucl. Phys.* **59** (2007) 147
[Lunn03] D. Lunney et al., *Rev. Mod. Phys.* **75** (2003) 1021
[May49] M Goeppert-Mayer, *Phys. Rev. C* **75** (1949) 1969
O. Haxel et al., *Phys. Rev. C* **75** (1949) 1766
[Moll85] P. Möller et al. *At. Data Nucl. Data Tables* **59** (1995) 185
[Moto95] T. Motobayashi et al., *Phys. Lett. B* **346** (1995) 9
[N8] H. Iwasaki et al., *Phys. Lett. B* **491** (2000) 8,
D.J. Millener et al., *Phys. Rev. C* **28** (1983) 497,
A. Navin et al., *Phys. Rev. Lett.* **85** (2000) 266,
S. Shimoura et al., *Phys. Lett. B* **654** (2007) 87.
[N20] X. Campi et al., *Nucl. Phys. A* **251** (1975) 193
A. Poves and J. Retamosa, *Phys. Lett. B* **184** (1987) 311
W. Warbutron, J.-A. Becker and B.A. Brown, *Phys. Rev. C* **41** (1990) 1147
[N40] M. Hannawald et al., *Phys. Rev. Lett.* **82** (1999)1391,
O. Sorlin et al., *Eur. Phys. J. A* **16** (2003) 55
[ngdp] F. Kaeppeler et al. *Ap. J.* **347** (1989) L43,
E. Kraussmann et al. *Phys. Rev. C* **53** (1996) 469,
L. Gaudefroy et al. *Eur. Phys. J. A* **27** (s01) (2006) 302,
O. Sorlin et al. *C. R. Phys.* **4** (2003) 541.
[Nota02] M. Notani et al., *Phys. Lett. B* **542** (2002) 49
[Nowa09] F. Nowacki and A. Poves, *Phys. Rev. C* **79** (2009) 014310
[NSCL] M. Fauerbach et al., *Phys. Rev. C* **53** (1996) 647
[Pfei01] B. Pfeiffer et al., *Nucl. Phys. A* **693** (2001) 282
[Porq09] M. G. Porquet, private communication
[Pove87] A. Poves and J. Retamosa, *Phys. Lett. B* **184** (1987) 311
[Rile08] L.A. Riley et al., *Phys. Rev. C* **78** (2008) 011303 (R)
[Otsu01] T. Otsuka et al., *Phys. Rev. Lett.* **87** (2001) 082502
[Otsu10] T. Otsuka et al., *Phys. Rev. Lett.* **104** (2010) 012501
[Otsu10b] T. Otsuka et al., arXiv : 0908.2607v2 [nucl-th] Jan 25th 2010
[Quin86] E. N. M. Quint et al., *Phys. Rev. Lett.* **57** (1986) 186
[Raus97] T. Rauscher et al., *Phys. Rev. C* **56** (1997) 1613
[Raus98] T. Rauscher et al., *Phys. Rev. C* **57** (1998) 2031
[Schw10] J. Holt, T. Otsuka, A. Schwenk, and T. Suzuki, private communication
[Schi07] A. Schiller et al., *Phys. Rev. Lett.* **99** (2007) 014316
[Smir10] N.A. Smirnova et al., *Phys. Lett. B* **686** (2010) 109, and Smirnova's lecture.
[Sne98] C. Sneden et al., *Ap. J.* **496** (1998) 235, and C. Sneden et al., *Ap. J.* **533** (2000) L139.
[Sorl08] O. Sorlin and M.-G. Porquet, *Prog. Part. Nucl. Phys.* **61** (2008) 602
[Sorl10] O. Sorlin, proceedings of the NN2009 conference, to be published in *Nucl. Phys. A*
[Stan09] M. Stanoiu et al., *Phys. Rev. C* **78** (2008) 034315
[Terr08] J. R. Terry et al., *Phys. Rev. C* **77** (2008) 014316
[Thib75] C. Thibault et al., *Phys. Rev. C* 12 (1975) 644
[Tru01] J.W. Truran et al., *Nucl. Phys.* ***A*** 688 (2001) 330c
[Utsu99] Y. Utsuno et al., *Phys. Rev. C* **60** (1999) 054315
[VlowK] S. K. Bogner, T. T. S. Kuo and A. Schwenk, *Phys. Rep.* **386** (2003) 1
[Warb90] W. Warburton, J. A. Becker and B. A. Brown, *Phys. Rev. C* **41** (1990) 1147
[Woos94] S. E. Woosley et al., *Astrophys. J.* **433** (1994) 229